# A Ruthenium(II) Complex Containing a Redox-Active Semiquinonate Ligand as Potential Chemotherapeutic Agent: From Synthesis to In Vivo Studies

Anna Notaro, Angelo Frei, Riccardo Rubbiani, Marta Jakubaszek, Uttara Basu, Severin Koch, Cristina Mari, Mazzarine Dotou, Olivier Blacque, Jeremie Gouyon, et al.

# A Ruthenium(II) Complex Containing a Redox-Active Semiquinonate Ligand as Potential Chemotherapeutic Agent: From Synthesis to *in vivo* Studies

*Anna Notaro,[a,#] Angelo Frei,[b,#] Riccardo Rubbiani,[b,#] Marta Jakubaszek,[a, e] Uttara Basu,[a] Severin Koch,[b] Cristina Mari,[b] Mazzarine Dotou,[a] Olivier Blacque,[b] Jérémie Gouyon,[c] Fethi Bedioui,[c] Nils Rotthowe,[d] Rainer F. Winter,[d] Bruno Goud,[e] Stefano Ferrari,[f,g] Mickaël Tharaud,[h] Martina Řezáčová,[i] Jana Humajová,[j] Pavel Tomšík,[i] and Gilles Gasser[a,*]*

[a] Chimie ParisTech, PSL University, CNRS, Institute of Chemistry for Life and Health Sciences, Laboratory for Inorganic Chemical Biology, F-75005 Paris, France.

[b] Department of Chemistry, University of Zurich, Winterthurerstrasse 190, 8057 Zurich, Switzerland.

[c] Chimie ParisTech, PSL University, CNRS, Institute of Chemistry for Life and Health Sciences, Team Synthèse, Electrochimie, Imagerie et Systèmes Analytiques pour le Diagnostic, F-75005 Paris, France.

[d] Department of Chemistry, University of Konstanz, Universitätsstrasse 10, D-78457 Konstanz, Germany.

[e] Institut Curie, PSL University, CNRS UMR 144, F-75005, Paris, France.

[f] Institute of Molecular Cancer Research, University of Zurich, CH-8057, Zurich, Switzerland.

[g] Institute of Molecular Genetics of the Czech Academy of Sciences, Videnska 1083, 143 00 Prague, Czech Republic.

[h] Université de Paris, Institut de physique du globe de Paris, CNRS, F-75005 Paris, France.

[i] Department of Medical Biochemistry, Faculty of Medicine in Hradec Kralove, Charles University, Šimkova 870, 500 03 Hradec Kralove, Czech Republic.

[j] Department of Medical Biochemistry, Faculty of Medicine in Prague, 150 06 Prague, Czech Republic.

[#] these authors have contributed equally to the work

* Corresponding author: E-mail: gilles.gasser@chimeparistech.psl.eu; WWW: www.gassergroup.com; Phone: +33 1 44 27 56 02

ORCID Number

Anna Notaro: 0000-0003-0148-1160

Angelo Frei: 0000-0001-6169-2491

Marta Jakubaszek: 0000-0001-7590-2330

Uttara Basu: 0000-0002-0509-2421

Mazzarine Dotou: 0000-0001-8781-6763

Olivier Blacque: 0000-0001-9857-4042

Fethi Bedioui: 0000-0002-0063-4412

Bruno Goud: 0000-0003-1227-4159

Stefano Ferrari: 0000-0002-6607-215X

Martina Řezáčová: 0000-0001-5370-2290

Jana Humajová (Mattová): 0000-0001-8099-6781

Pavel Tomšík: 0000-0002-4366-075X

Gilles Gasser: 0000-0002-4244-5097

**Keywords:** Bioinorganic Chemistry, Cancer, DNA, Medicinal Inorganic Chemistry, Ruthenium.

**Abstract**

Chemotherapy remains one of the dominant treatments to cure cancer. However, due to the many inherent drawbacks, there is a surge for new chemotherapeutic drugs. Many classes of compounds have been investigated over the years in order to discover new targets and synergistic mechanisms of action including multicellular targets. In this work, we designed a new chemotherapeutic drug candidate against cancer, namely $[Ru(DIP)_2(sq)]PF_6$ (**Ru-sq**) (DIP = 4,7-diphenyl-1,10-phenanthroline; sq = semiquinonate ligand). The aim was to combine the great potential expressed by Ru(II) polypyridyl complexes and the singular redox and biological properties associated to the catecholate moiety. Experimental evidences (e.g. X-ray crystallography, electron paramagnetic resonance, electrochemistry) demonstrate that the semiquinonate is the preferred oxidation state of the dioxo ligand in this complex. The biological activity of **Ru-sq** was then scrutinised *in vitro* and *in vivo*, and the results highlight the auspicious potential of this complex as a chemotherapeutic agent against cancer.

## Introduction

In the last decades, the search for new chemotherapeutic agents against cancer has challenged scientists worldwide. Chemotherapy, together with surgery, radiotherapy and immunotherapy, is used in a combined modality therapy to treat cancer.[1] The goal of this combination is to overcome the drawbacks of each singular treatment to afford the best chances of survival for the patients.[1] Cisplatin is one of the most common chemotherapeutic agents utilized against cancer. However, its severe side effects are limiting its clinical use.[2–6] Therefore, many other platinum-based drug candidates have been investigated over the last 40 years leading to the worldwide clinical approval of carboplatin and oxaliplatin.[7,8] On the basis of these ground-breaking discoveries and the observed occurrence of resistance with platinum treatment, a large number of metal complexes based on other metals than platinum have been examined.[9–18] In this field, ruthenium complexes play a central role due to their inherent advantages (e.g., multiple stable oxidation states, well-established chemistry, etc.).[19–23] Interestingly, Ru(III) and Ru(II) complexes usually have ligand exchange kinetics similar to those of Pt(II) complexes.[19] In addition, ruthenium complexes have found applications in different fields of medicinal chemistry against cancer since they behave differently depending on the biological settings, therefore displaying different biological targets.[24–29] KP-1019, IT-139 (formerly NKP-1339) and NAMI-A are, to date, the only three Ru complexes to have reached clinical trial as anticancer agents. Their mechanism of action involves ligand exchange, resembling therefore the one of cisplatin.[30–35] Of note, TLD-1433, a substitutionally inert Ru(II) polypyridyl complex, has recently entered phase II clinical trial as a photosensitizer for photodynamic therapy (PDT).[36,37] Another very promising class of ruthenium complexes are the coordinatively saturated and substitutionally inert ruthenium polypyridyl complexes. These compounds have been

intensely investigated over the last years and several applications as potential chemotherapeutic agents have been unearthed.[24] At first, most of the bio-activity of these compounds was associated with interactions with DNA.[38–41] However, over the years, many other modes of action were identified, such as the trigger of mitochondrial dysfunction,[42–44] Topoisomerases I and II inhibition,[45,46] modification of cell membranes[47] and others.[24] Due to the great opportunities offered by this class of Ru compounds, in this work, we designed a new Ru polypyridyl complex, namely $[Ru(DIP)_2(sq)](PF_6)$ (**Ru-sq**, Scheme 1a) where DIP is 4,7-diphenyl-1,10-phenanthroline and sq is a semiquinonate ligand, which was found to be a very interesting anticancer drug candidate. Semiquinonate is a so-called 'non-innocent' ligand as its electrochemical properties strongly resemble that of the metal center.[48] Semiquinonate is the oxidised form of catechol, a well-known dioxo ligand, which can exist in three redox forms, namely catecholate (cat), semiquinonate (sq) and quinone (q) (Scheme 1b).[49] Catecholate and its oxidation products have already been intensively investigated as ligands.[50,51] However, the focus of these studies has mostly been on the unique electronic/redox properties of metal complexes containing such 'non-innocent' dioxo ligands.[52–55] Catechols are also known as pan-assay interference compounds (PAINS) due to their redox and chelating properties.[56] Nevertheless, catecholate and its derivatives have also shown potential in different fields of biological interest,[57–61] such as cancer chemoprevention,[59] antifungal activity[60] and the inhibition of the spontaneous Aβ fibril formation,[61] which is a key target for the treatment of Alzheimer´s disease. Worthy of note, vanadium compounds carrying catechol-like ligands have been investigated by Crans and co-workers.[62,63] During these studies, particularly potent cytotoxic vanadium (V) catecholate complexes toward bone cancer cells were unveiled.[62] The cytotoxicity on glial cells of $[Ru^{III}(NH_3)_4(catecholate)]^+$ was also

investigated in 2007 by Almeida and co-workers.[58] In this case, the catechol was found to be more cytotoxic than the Ru(III) complex itself with an $EC_{50}$ of 0.342 mM against rat astrocytes and 0.568 mM against human glioblastoma GL-15 cell line, while the $[Ru^{III}(NH_3)_4(catecholate)]^+$ complex had $EC_{50}$ = 1.380 mM and $EC_{50}$ = 2.6 mM against rat astrocytes and human glioblastoma, respectively.[58] Further studies suggested that depletion of glutathione and induction of apoptosis were possible explanations for the cytotoxicity observed for catechol towards mouse neuroblastoma N2a cell line.[57] These preliminary studies rationalize our choice to integrate catechol and its oxidation products into a Ru(II) polypyridyl complex. To the best of our knowledge, $[Ru(DIP)_2(sq)](PF_6)$ is the first Ru(II) polypyridyl complex containing a catechol moiety to be deeply investigated from both a physico-chemical and biological point of view. The complex was isolated as a racemic mixture of Δ and Λ enantiomers. No effort was made in this work to isolate pure enantiomers. As described below, *in vitro* and *in vivo* studies demonstrate a significant potential of this compound as a chemotherapeutic agent against cancer.

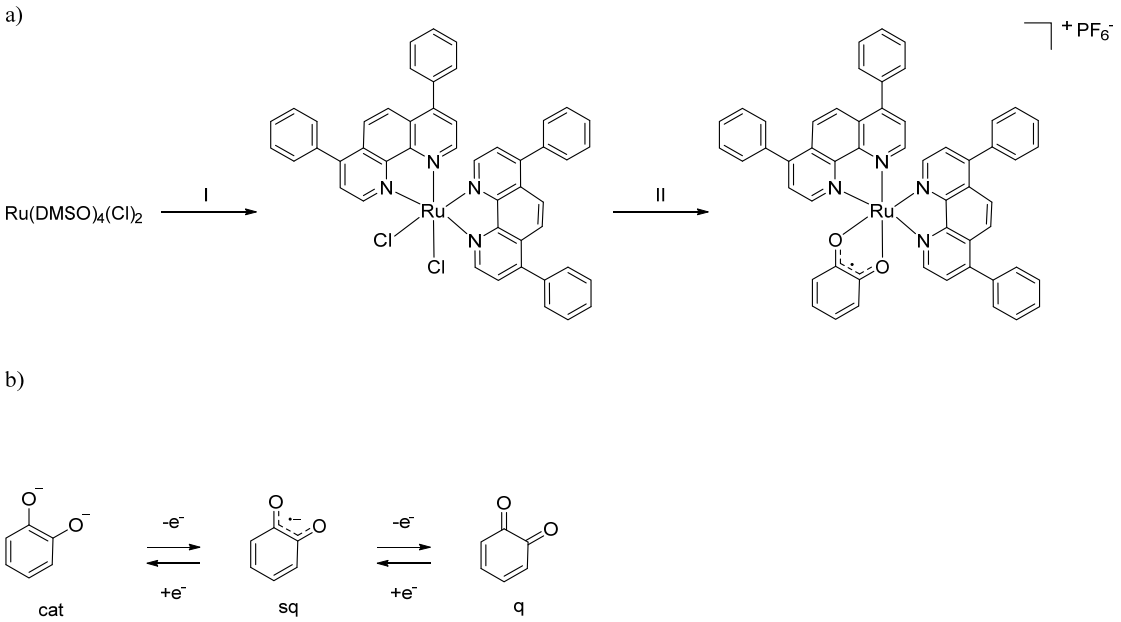


**Scheme 1.** a) Synthesis of **[Ru(DIP)$_2$(sq)](PF$_6$)**. I) DIP, LiCl, DMF, reflux, 24 h, 78%; II) (i) NaOH, catechol 2-propanol, reflux, 24h; (ii) air, 2 h; (iii) $NH_4PF_6$, 2-propanol/$H_2O$ (1:8), 19%. b) Catecholate (cat) and its oxidised forms, semiquinonate (sq) and quinone (q).

## Results and Discussion

### Synthesis and characterization of [Ru(DIP)$_2$(sq)](PF$_6$)

The synthesis of the target compound **[Ru(DIP)$_2$(sq)](PF$_6$)** was achieved in a 2-step synthesis (Scheme 1a). Briefly, the known $Ru(DMSO)_2Cl_2$[64], DIP and LiCl were refluxed in DMF to afford $Ru(DIP)_2Cl_2$ in 72% yield after precipitation with acetone.[65] The compound was then refluxed in a nitrogen atmosphere overnight with catechol in the presence of NaOH in 2-propanol. The oxidation step of the catecholate to the semiquinonate was performed by exposing the solution of the Ru complex in 2-propanol to air for 2 h. $[Ru(DIP)_2(sq)](PF_6)$ was obtained in 19% yield after precipitation with a large excess of $NH_4PF_6$ and purification *via* silica gel chromatography. The identity of the product was confirmed by HR-MS and NMR spectroscopy. $^1$H-NMR spectra showed a characteristic peak broadening in the aromatic

region between 7–9 ppm due to the paramagnetism of the complex. In the $^{13}C$ NMR and 2D $^{1}H$-$^{13}C$ HSQC spectra (Figure S1) ten inequivalent *C*H carbons were observed. The purity of the product was confirmed by microanalysis.

**X-ray Crystallography of [Ru(DIP)$_2$(sq)](Cl)**

The crystal structure of [Ru(DIP)$_2$(sq)](Cl) was determined by a single crystal X-ray diffraction study. Suitable single crystals were grown from slow diffusion of diethylether into a solution of the product prior to precipitation with $NH_4PF_6$ in MeCN. The crystal structure revealed two independent Ru molecules (Ru-1 and Ru-2 in Figure S2), two chloride counter ions (from LiCl) and three water molecules in the asymmetric unit (monoclinic $P2_1/c$ space group). Both Cl atoms are disordered over two sets of sites with site-occupancy ratios of 0.299/0.701(3) and 0.244/0.756(5). The H atoms of the isolated water molecules could be introduced in the final refinements, but their positions were kept fixed to satisfy reliable hydrogen bonding. The molecular structure of one of the independent Ru molecules is shown in Figure 1 and a selection of the most relevant bond lengths and angles are provided in Tables S1 and S2 (additional crystallographic information can be found in the supporting information). The X-ray crystal structure determination also provided evidence for the nature of the dioxo ligand, as it can exist as catecholate, semiquinonate and quinone.[49,53,66] The typical range for the C-O bond length of such a ligand coordinated to a metal is 1.34–1.47 Å for the catecholate form, 1.27–1.31 Å for the semiquinonate form and around 1.23 Å for the quinone.[49,66] The C-O bond distances of the dioxo ligand in [Ru(DIP)$_2$(sq)](Cl) are 1.309(4), 1.314(4), 1.315(4) and 1.319(4) Å, which suggest that it is present in its semiquinonate form.[49]

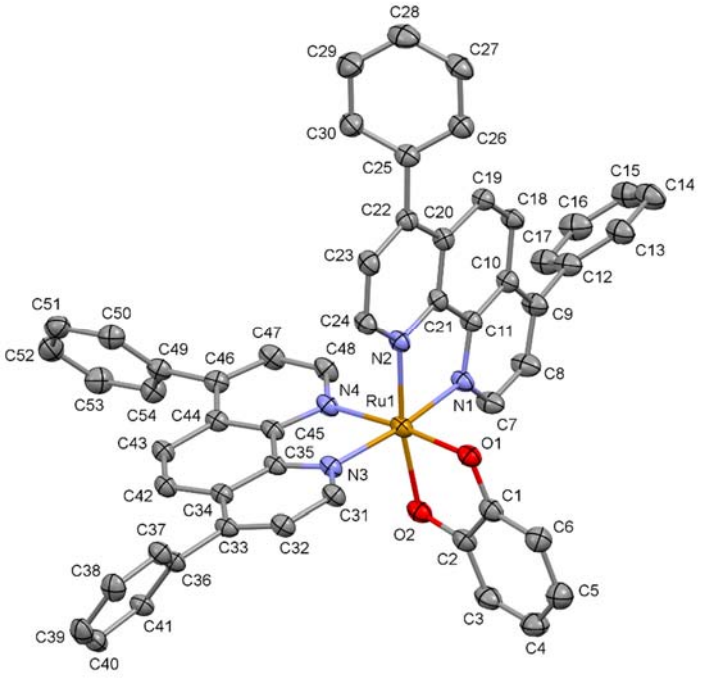


**Figure 1.** Molecular structure of [Ru(DIP)$_2$(sq)](Cl). The asymmetric unit contains two crystallographically independent Ru cations, only one of which is presented. The $Cl^-$ counter ions, H atoms and solvent molecules are omitted for clarity. The thermal ellipsoids are shown at the 30% probability level.

**Electrochemistry**

The electrochemistry of **[Ru(DIP)$_2$(sq)](PF$_6$)** (abbreviated as **Ru-sq**) was investigated using cyclic voltammetry (CV) and rotating disc electrode voltammetry (RDE) in DMF containing tetrabutylammonium hexafluorophosphate 0.1 M. The RDE voltammogram shown in Fig. S3 exhibits four well-defined, reversible waves, in addition to that of decamethylferrocene, which was used as internal reference with a half-wave potential of 0.030 V *vs* the Saturated Calomel Electrode (SCE). The four features related to the **Ru-sq** have the same intensity, which attests that the related redox processes involve the same number of exchanged electrons. By comparison with the data reported in the literature for closely related complexes under similar conditions,[52,67,68] the underlying redox processes were assigned as shown in Table S3. The oxidation located at + 0.647 V vs SCE can be attributed to the Ru(II)/Ru(III) redox couple while the sq/cat redox

couple can be associated to the first reduction process at -0.249 V vs SCE. The following two processes, at more negative potentials, can be assigned to the sequential reductions of the ancillary ligands ($DIP^{0/-}$). Of note, the latter are separate couples with quite some substantial redox splitting.[52,67] These data clearly show how the presence of the semiquinonate ligand influences the redox properties of the metal centre, causing a shift to lower potential. The couple of Ru (III)-quinone ligand is not observed in these conditions since they are possibly located outside the anodic limit of a DMF-based electrolyte. Moreover, the CV experiment (Figure S3) indicates the reversibility of the redox processes, at least on the voltammetric timescale.

**Electron Paramagnetic Resonance**

**Ru-sq** in its native state is Electron Paramagnetic Resonance (EPR) active in DCM due to the presence of an unpaired spin as already confirmed by X-ray crystallography (Figure S4a). At room temperature, a rather broad isotropic signal was observed. Its *g*-value of 2.0244 is in line with a ligand-centred spin density and deviates only slightly from the free electron value $g_e$ of 2.0023. This behaviour is in strong contrast to a metal-centred spin of a Ru(III) complex, which would only become observable at low temperatures due to rapid relaxation and display a broad, axial or rhombic signal with large anisotropy.[53,69] The reduced form **Ru-cat** (Scheme 2) was generated by the reaction of **Ru-sq** with equimolar amounts of cobaltocene ($Cp_2Co$, $E_{1/2}$ = -0.880 V vs SCE in DMF/0.1 M $NBu_4PF_6$) (Figure S4b).[70] Owing to the presence of a low-spin Ru(II) ion and a closed-shell catecholate ligand this species is EPR silent. The same holds also true for oxidized, dicationic **$Ru^+$-sq** (Scheme 2), which was prepared by treatment of **Ru-sq** with an excess of 1,1'-diacetylferrocenium hexafluoroantimonate ($Ac_2FcSbF_6$, $E_{1/2}$ = 0.940 V vs SCE in DMF/0.1 M $NBu_4PF_6$) (Figure S4c).[70,71] The

absence of an EPR signal indicates that the unpaired spins at the Ru(III) ion (**Ru**$^{+}$) and the sq ligand are antiferromagnetically coupled.

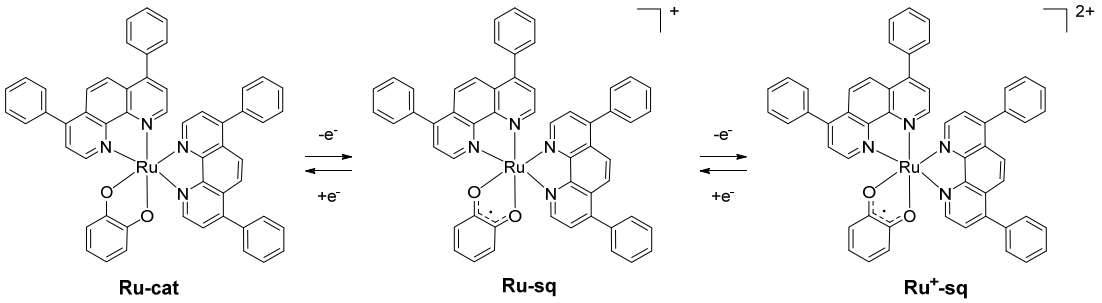


**Scheme 2.** Structures of **Ru-cat**, **Ru-sq**, and **Ru**$^{+}$**-sq,** carrying a catecholate or a semiquinonate ligand and Ru in oxidation state +II (**Ru**) or +III (**Ru**$^{+}$), respectively.

**Stability in DMSO and human plasma**

The stability of a compound plays an important role in its biological activity and viability. Therefore, the integrity of **Ru-sq** was first assessed in DMSO-d$^{6}$ using $^{1}$H NMR spectroscopy. **Ru-sq** was found to be stable in DMSO over 8 days. No change in the NMR spectra of the complex was observed over 8 days (Figure S5). Next, to obtain a preliminary insight into the behaviour of **Ru-sq** under physiological conditions, the stability of **Ru-sq** in human plasma was investigated by UPLC following a procedure already established by our group.[43] **Ru-sq** was incubated in human plasma at 37°C for 0 h, 4 h, 6 h, 12 h, 20 h and 24 h using diazepam as an internal standard. The UV traces of the UPLC analysis are shown in Figure S6a. The concentration of **Ru-sq** was normalized with respect to the internal standard and plotted against time. The linear trend shown in Figure S6b clearly demonstrates that between 6 and 20 h, a decomposition of 50% of the compound was observed, to reach a total degradation of the compound after 24 h.

## Cytotoxicity Studies

After a full characterisation of **Ru-sq**, its potential activity as a chemotherapeutic agent was investigated starting from the biological evaluation of its behaviour against cancer cells in monolayer cell cultures. The cytotoxicity of **Ru-sq** towards HeLa (human cervical adenocarcinoma), A2780 (human ovarian carcinoma), A2780 cis (human cisplatin resistant ovarian carcinoma), A2780 ADR (human doxorubicin resistant ovarian carcinoma), CT-26 (mouse colon adenocarcinoma), CT-26 LUC (mouse colon adenocarcinoma stably expressing luciferase), RPE-1 (human normal retina pigmented epithelial) and MRC-5 (human normal lung fibroblast) cell lines was therefore investigated using a fluorometric cell viability assay (single graphs available in Figures S7).[72] Cytotoxicity of cisplatin and doxorubicin was determined in the same cell lines as positive controls and, as additional controls, **Ru(DIP)$_2$Cl$_2$** and catechol were also tested.[73,74] As shown in Table 1 where $IC_{50}$ (the half maximal inhibitory concentration) values are reported, **Ru-sq** displayed $IC_{50}$ values between the high nanomolar and low micromolar range on the cell lines investigated in this study, while the **Ru(DIP)$_2$Cl$_2$** precursor and the catechol ligand itself showed much lower cytotoxicity. Very impressively, **Ru-sq** exerted an activity 40 times higher than cisplatin against a cisplatin resistant cell line. On the other hand, the cytotoxicity of doxorubicin and **Ru-sq** against a doxorubicin resistant cell line appeared to be in the same order of magnitude. Overall, complex **Ru-sq** displays a cytotoxicity, which is comparable to doxorubicin and much higher than the one of cisplatin. However, no selectivity was observed between cancerous and non-cancerous cell lines. This shortcoming is often faced in medicinal chemistry and could be improved by the introduction of a targeting moiety or by nanoformulation.

**Table 1.** $IC_{50}$ values of **Ru-sq**, the **$Ru(DIP)_2Cl_2$** precursor and the catechol ligand in tested cell lines; cisplatin and doxorubicin were used as positive controls.

| **$IC_{50}$ (μM)** | **HeLa** | **A2780** | **A2780 ADR** | **A2780 cis** | **CT-26** | **CT-26 LUC** | **RPE-1** | **MRC-5** |
|---|---|---|---|---|---|---|---|---|
| **Cisplatin** | 9.28 ± 0.20 | 4.00 ± 0.76 | 8.32 ± 0.71 | 18.33 ± 2.92 | 2.60 ± 0.18 | 2.42 ± 0.23 | 30.24 ± 5.11 | 11.20 ± 2.32 |
| **Doxorubicin** | 0.34 ± 0.02 | 0.19 ± 0.03 | 5.94 ± 0.58 | 0.54 ± 0.04 | 0.082 ± 0.003 | 0.18 ± 0.006 | 0.89 ± 0.17 | 3.37 ± 1.24 |
| **Ru-sq** | 0.50 ± 0.01 | 0.67 ± 0.04 | 4.13 ± 0.2 | 0.45 ± 0.03 | 1.00 ± 0.03 | 1.51 ± 0.14 | 0.90 ± 0.04 | 0.95 ± 0.09 |
| **$Ru(DIP)_2Cl_2$** | 15.03 ± 0.4 | 4.69 ± 0.14 | 78.27 ± 4.9 | 6.36 ± 0.57 | 9.20 ± 1.22 | 6.65 ± 0.5 | 3.13 ± 0.07 | 5.54 ± 0.39 |
| **Catechol** | >100 | 22.80 ± 5.96 | >100 | 54.55 ± 11.30 | 16 ± 4.14 | 11.56 ± 0.40 | >100 | >100 |

We then decided to pursue the investigation of **Ru-sq** behaviour in a Multi Cellular Tumour Spheroids (MCTS) model.[75] It was previously shown that such a model mimics the *in vivo* microenvironment and tumour metabolism.[76,77] Moreover, large MCTS develop a central necrosis core similar to that found in the inner core of tumours.[78] These unique features give a better representation of a cancer model compared to a 2D model, lowering the disparity between *in vitro* and *in vivo* models.[78] Table 2 shows the $IC_{50}$ values obtained *via* a luminescent cell viability assay for compounds that were administered to HeLa MCTS for 48 h (single graphs are availabe in Figure S8). The **$Ru(DIP)_2Cl_2$** precursor and the catechol ligand were tested as additional controls and exhibited lower cytotoxicity than **Ru-sq**. Catechol showed no toxicity towards the cell line tested ($IC_{50}$ > 100 μM) while the precursor displayed a cytotoxicity comparable to cisplatin. Cisplatin was used as a positive control and the results are in line with literature data.[79] The cytotoxicity of **Ru-sq** in HeLa MCTS was impressively high after 48 h treatment, with $IC_{50}$ ~ 14 μM, which is 3 times lower than cisplatin or doxorubicin

($IC_{50}$ ~ 47 μM or 39 μM, respectively). Noteworthy, the cytotoxicity of **Ru-sq** was comparable to the one of doxorubicin after 72 h treatment ($IC_{50}$ ~ 11 μM).[80] These studies clearly demonstrate the high potential of **Ru-sq** as an anticancer drug candidate. The impressive bioactivity, comparable to doxorubicin in monolayer cell culture, was also confirmed in the 3D tumour model – HeLa MCTS.

**Table 2.** $IC_{50}$ values for **Ru-sq**, **$Ru(DIP)_2Cl_2$** precursor and the catechol ligand in multicellular HeLa cancer cell spheroids (approximately 400 μm in diameter); cisplatin and doxorubicin were used as positive controls.

| **$IC_{50}$ (μM)** | **Cisplatin** | **Doxorubicin** | **Ru-sq** | **$Ru(DIP)_2Cl_2$** | **Catechol** |
|---|---|---|---|---|---|
| **HeLa MCTS** | 46.49 ± 4.18 | 38.59 ± 0.43 | 14.11 ± 0.09 | 59.84 ± 3.05 | >100 |

Spheroid integrity and growth upon treatment are very useful tools to determine a potential drug activity.[78] In this study MCTS were monitored over 13 days after treatment with different concentrations of **Ru-sq** (Figure 2). Every 3 days, the spheroids were washed to remove dead cells and their diameters were measured (Figure 2). It is important to note that at each washing step, half of the media was removed and replaced with fresh one, diluting twice the quantity of the compound in each well. The effect of **Ru-sq** on growth inhibition is dose-dependent and already visible after 3 days. Low concentrations treatments (1 μM and 2.5 μM) led to regrowth of the spheroids after the first 72 h, while for 5 μM and 10 μM treatments, the regrowth is visible after 6 and 9 days, respectively. **Ru-sq** treatment with concentrations higher than $IC_{50}$ (20 μM and 25 μM) completely inhibits the spheroids growth after 13 days of treatment. Overall, we can conclude that **Ru-sq** treatment at 20 μM and 25 μM concentrations, severely affect the size and the integrity of the spheroids after 13 days of treatment.

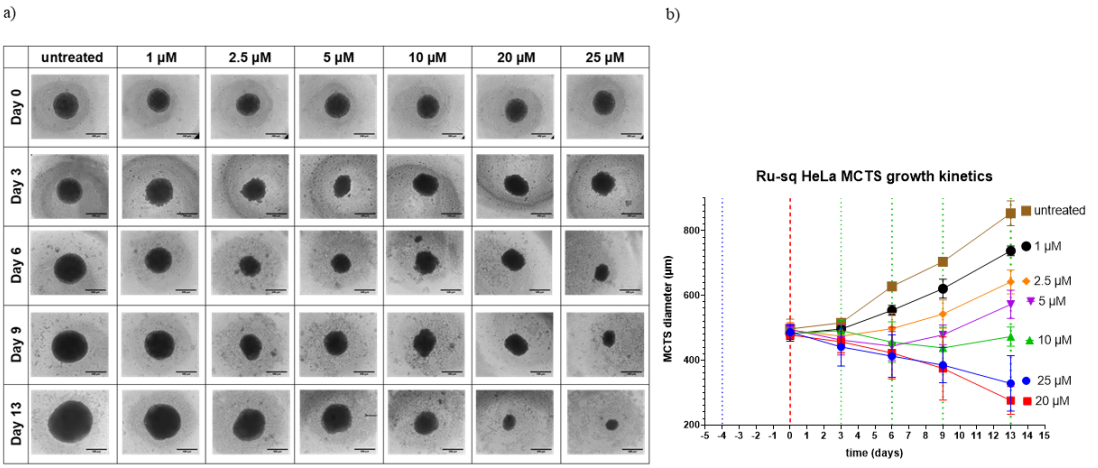


**Figure 2.** Growth kinetics of HeLa MCTS upon treatment with different concentrations of **Ru-sq** (1, 2.5, 5, 10 and 20 µM). a) Images collected at day 0 (before treatment) and at day 3, 6, 9 and 13. b) MCTS diameter calculated at different time points. Blue dotted line indicates day of seeding, red dashed line indicates day of treatment, green dotted lines indicate days of washing.

## Cell Death Mechanism

The excellent activity displayed by **Ru-sq** in HeLa MCTS encouraged us to perform further experiments in order to obtain more insights into its *in vitro* behaviour. The first step was the evaluation of the type of cell death occurring when cancer cells were treated with **Ru-sq**. For this experiment, HeLa cells were analysed *via* flow cytometry using the Annexin V and PI (propidium iodide) staining method.[81] Staurosporine, a known inducer of apoptosis, was employed as a positive control.[82] As shown in Figure 3 and Figure S9 (dot plots), **Ru-sq** induced significant apoptosis as early as 30 min treatment with progression from early to late apoptosis at 4 h. The level of apoptosis induction by the complex after 4 h was comparable to that caused by 24 h staurosporine treatment. These data clearly demonstrate that **Ru-sq** induces apoptosis as the only type of cell death in HeLa cells.

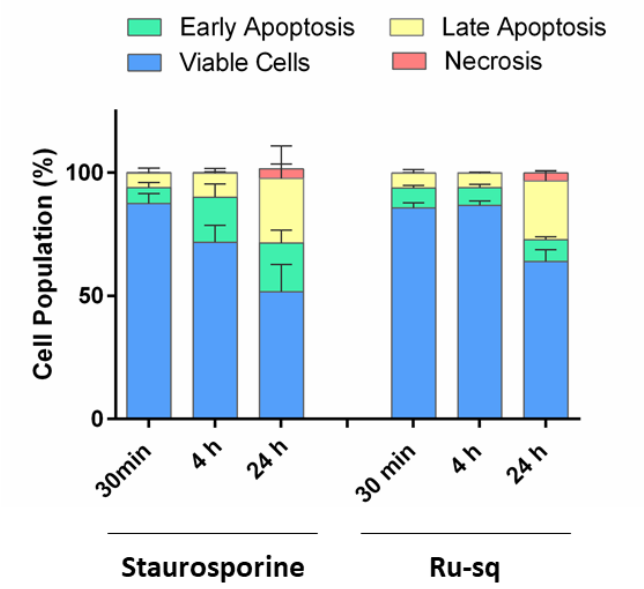


**Figure 3.** Induction of apoptosis/necrosis in HeLa cells upon treatment with **Ru-sq** (10 μM) and staurosporine (1 μM) at different time frames. The values are expressed as a mean ± S.D. (standard deviation) of three biological repeats.

**Cellular uptake, intracellular distribution and DNA metalation studies**

Next, the cellular uptake of **Ru-sq** and cisplatin was investigated in HeLa cells. The amount of ruthenium accumulated was detected by Inductively Coupled Plasma Mass Spectrometry (ICP-MS). Working concentrations and incubation times were chosen to avoid extended cell mass loss due to the high cytotoxicity of the complexes but considering a ruthenium final amount that could afford determination of the metal content. After 2 h treatment (5 μM), **Ru-sq** internalises slightly better than the drug cisplatin (Figure 4a**)**. The low accumulation of cisplatin in these working conditions is in agreement with the literature data.[83,84] To have more insights about uptake mechanisms of **Ru-sq** into the HeLa cells, additional experiments were performed. Cells were pre-treated with different inhibitors of uptake pathways or kept at different

temperatures to assess the energy dependence of the uptake mechanism(s) (Figure S10). More specifically, low temperature (4ºC), pre-treatment with metabolic inhibitors (which decreases ATP production), pre-treatment with chloroquine or ammonium chloride (which mostly impede endocytic pathways), or pre-treatment with tetraethylammonium chloride (mostly inhibiting cation transporters) decreased **Ru-sq** accumulation in cells by half when compared to 37 ºC condition (see Figure S10). This outcome indicates that **Ru-sq** might be transported into the HeLa cells by both energy dependent (active) and energy independent (passive) pathways. Further cellular fractionation experiment showed preferential accumulation of **Ru-sq** inside the nucleus (Figure 4b). These findings suggest that the mode of action could be related to the damage caused to DNA and/or to prevention of replication as well as transcription.[85,86] In order to identify DNA as a potential target for the complex, the genetic material was extracted from HeLa cells after 2 h treatment with **Ru-sq** or cisplatin and the amount of metal analysed by ICP-MS. The DNA of cells treated with **Ru-sq** displayed a metal content much higher when compared to cisplatin. Taken together, these findings strongly suggest direct interaction with DNA as a possible mechanism of action exerted by **Ru-sq**.

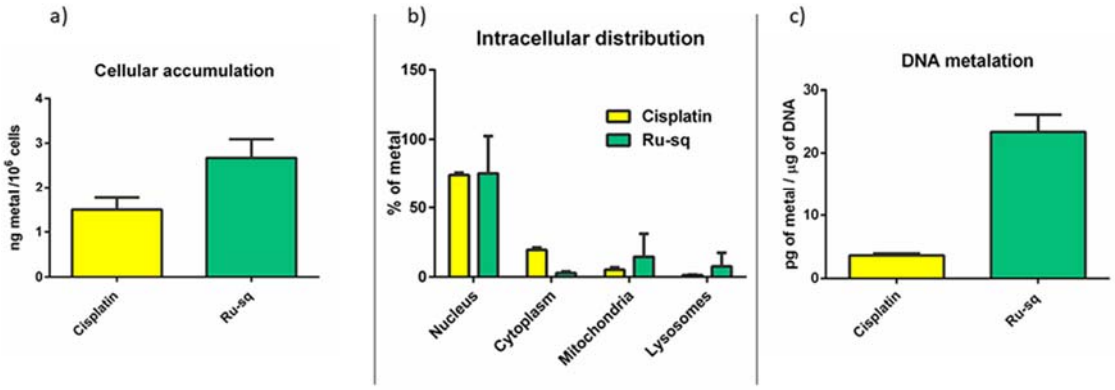


**Figure 4.** Cellular uptake (a), cellular fractionation (b) and DNA metalation (c) of HeLa cells after treatment with tested compounds (5 µM, 2 h). Data are presented as the mean ± SD of at least 3 biological replicates.

**JC-1 Mitochondrial Membrane Potential Test and Metabolic Studies**

The search for additional mechanisms of action associated to the treatment of **Ru-sq** led us to the investigation of the mitochondrial metabolism impairment.[87] Firstly, the mitochondrial membrane potential was studied with the use of a largely used indicator JC-1 (a membrane-permeant dye).[88,89] At high potentials, the dye forms red emitting aggregates in the mitochondria membrane, whereas at low potentials, it stays as a green emitting monomer.[88,89] The membrane potential is directly connected to oxidative phosphorylation (the main mitochondrial function).[90] HeLa cells were treated for 24 h with increasing concentrations of **Ru-sq** (from 0.2 µM to 0.6 µM). Figure 5a shows a slight decrease of the red fluorescence signal with increasing concentrations of **Ru-sq** and a significant drop in the signal around the $IC_{50}$ concentration (0.5 µM, marked in red). However, the dramatic collapse of mitochondrial membrane potential could also be caused by ongoing apoptosis.[91] Carbonyl cyanide 4-(trifluoromethoxy)phenylhydrazone (FCCP), an uncoupling agent that impairs the

membrane potential[92] was used as positive control.[92] Comparison of the results obtained with **Ru-sq (**0.5 μM) and FCCP treatment showed that the same loss in potential was detected. These findings strongly suggest a contribution of the membrane potential impairment to the cell death mechanism.

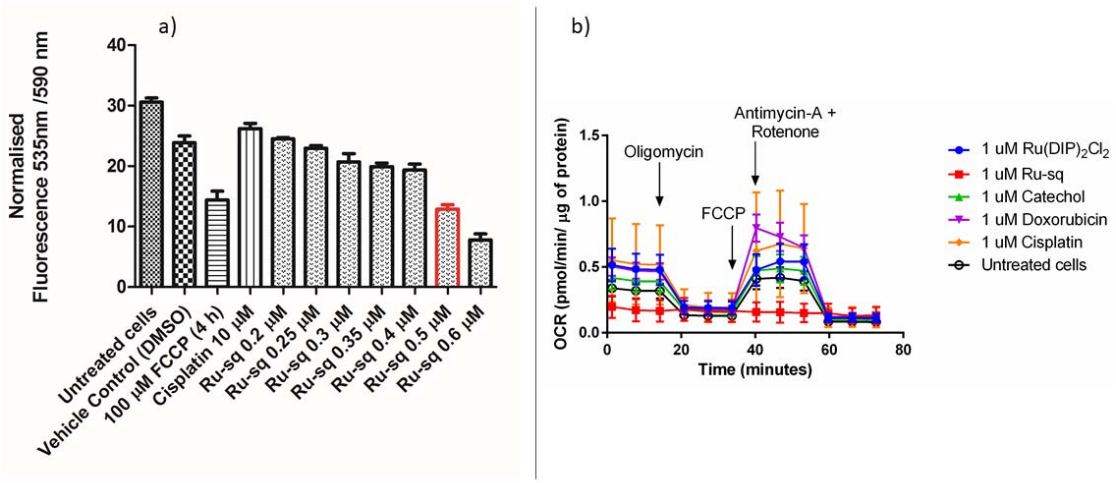


**Figure 5**. a) Fluorescence signal of JC-1 dye detected in HeLa cells treated for 24 h with different concentrations of **Ru-sq** (from 0.2 μM to 0.6 μM). Bar marked in red indicates the $IC_{50}$ concentration (0.5 μM). FCCP is used as positive control, cisplatin and DMSO (1%) are used as negative controls. b) Mito Stress Test profile in HeLa cells after 24 h treatment; oxygen consumption rate changes after treatment with specific electron transport chain inhibitors. Oligomycin (inhibitor of ATP synthase (complex V)), FCCP (uncoupling agent), Antimycin-A (complex III inhibitor) and Rotenone (complex I inhibitor).

Inspired by these findings, further studies on the metabolic pathways that could be affected by the complex were performed. For this purpose, Seahorse XF Analyzer was used to measure, in real time, the oxygen consumption rate (OCR) and extracellular acidification rate (ECAR) of treated cells. Firstly, the effect of **Ru-sq** on the oxidative phosphorylation in the HeLa cell line was investigated. Mitochondrial respiration was

found to be severely impaired in cells treated with **Ru-sq** as opposed to the precursor $Ru(DIP)_2Cl_2$. This was evident from the low basal respiration and the inhibition of ATP production compared to untreated cells. The mitochondrial membrane of the cells treated with **Ru-sq**, lost the capacity to restore the proton balance when treated with an uncoupling agent (FCCP). The maximal respiration (the OCR value when the mitochondrial membrane is uncoupled) and spare respiratory capacity (difference in the OCR values between maximal respiration and basal respiration) of the cells was reduced compared to untreated cells (Figure 5b and Figure S11). The combination of these effects suggests disrupted mitochondrial respiration in cervical cancer cells caused by **Ru-sq**. The effect on glycolysis and the possible metabolic modulation of the three primary fuel pathways (involving glucose, glutamine or fatty acids as substrates) were then examined. In contrast to that was observed for the mitochondrial respiration, the cell glycolysis, which is a cytosolic process, was not affected by **Ru-sq** (Figure S12). Additionally, due to the very low oxygen consumption rate in cells treated with **Ru-sq**, a direct effect on the 3-primary fuel pathways could not be determined (Figure S13). Overall, metabolic studies showed that the accumulation of **Ru-sq** in mitochondria has a significant role in the impairment of oxidative phosphorylation. This effect, together with the results obtained by the JC-1 staining, strongly suggests mitochondrial dysfunction as one of the modes of action of **Ru-sq**. In contrast, the chemotherapeutic drug cisplatin showed no significant effect on the mitochondrial metabolism of HeLa cells. This data suggests fundamental differences between the mode of action of **Ru-sq** and cisplatin. The latter covalently binds to the nuclear DNA and inhibits the replication process. It is widely known that DNA crosslinks can be repaired by different mechanisms such as the nucleotide excision repair (NER) that eventually leads to drug resistance in cancer cells. **Ru-sq**, with its multiple cellular

targets, could potentially evade these repair pathways and circumvent such drawbacks associated with cisplatin.

### *In vivo* efficacy studies

It is very difficult to evaluate selectivity of the anticancer drugs *in vitro*, as the proliferation of non-malignant cells is greatly affected by non-physiological conditions of cell culture in 2D and 3D models. The promising results obtained in studies conducted *in vitro* justified the assessment of **Ru-sq** efficacy in the context of whole organism. To this end, we performed *in vivo* studies to evaluate the effect on both tumour growth and survival of tumour-bearing mice. The doses were selected according to the dose-finding study, which had revealed a maximum tolerated dose (MTD) of 15 mg/kg of body weight. Two distinct models for testing *in vivo* efficacy of antitumor drugs are possible: a syngeneic (mice) tumour growing in a naturally immunocompetent mouse, or human tumour cells growing in immunodeficient animals. As both approaches have its advantages and pitfalls, we decided to use both models in this study.

### Effect of Ru-sq on the growth of Ehrlich mammary carcinoma in immunocompetent NMRI mice and survival of tumour bearing mice

Even though the use of syngeneic tumour allografts in naturally immunocompetent animals had been often considered inferior during the era of athymic mice models, this method made a comeback as the necessity of diversified, near-physiological experimental sets was recognised. In this model, we can observe the effect of the tested compound within the context of the genuine immune system that plays a key role in tumour resistance.[93]

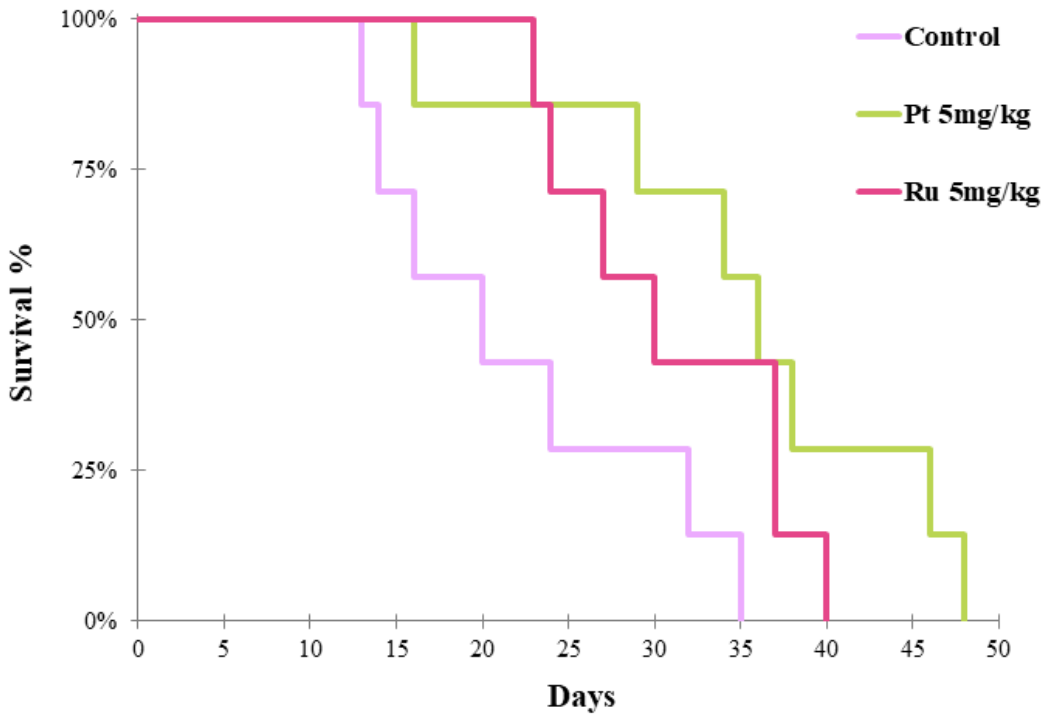


**Figure 6.** Kaplan-Meier analysis of survival of immunocompetent NMRI mice bearing Ehrlich carcinoma. Only the administration of complex **Ru-sq** 5 mg/kg i.p. and that of cisplatin (5 mg/kg) significantly prolonged the survival of tumour bearing mice when compared with the mixture of co-solvent and water. The compounds were administered i.p. on days 1 and 7 after tumour inoculation, n = 7 in each group.

During the study of the effect on the survival of immunocompetent NMRI mice bearing Ehrlich carcinoma (Figure 6), it was observed that the geometric mean of the overall survival of tumour bearing mice without therapy was 20.6 days. Among the three doses of **Ru-sq** tested, only 5 mg/kg prolonged the survival time significantly when compared with untreated tumour-bearing control mice (geom. mean = 31.9 days, $P = 0.033$). 10 mg and 15 mg/kg of **Ru-sq** seemed to exceed the optimal dose, causing a non-significant prolongation of survival ($P > 0.05$), with the geometric means of 30.2 and 25.5 days, respectively. The explanation may be a subclinical toxic effect that

negatively affects immune surveillance as well as other body functions necessary for the natural cancer defence. Although the optimal intracellular cancer-suppressing concentration may correspond to higher doses, subtle systemic toxicity does not allow to develop the desirable effect in vivo. The positive control cisplatin appeared to have similar efficacy (geom. mean = 33.7 days, *P* 0.014). An interesting and rare phenomenon was observed in all three groups of **Ru-sq**. Although the tumour was advanced in the later stage of the experiment, all mice treated with **Ru-sq** showed active behaviour, little cachexia and unsuppressed food consumption.

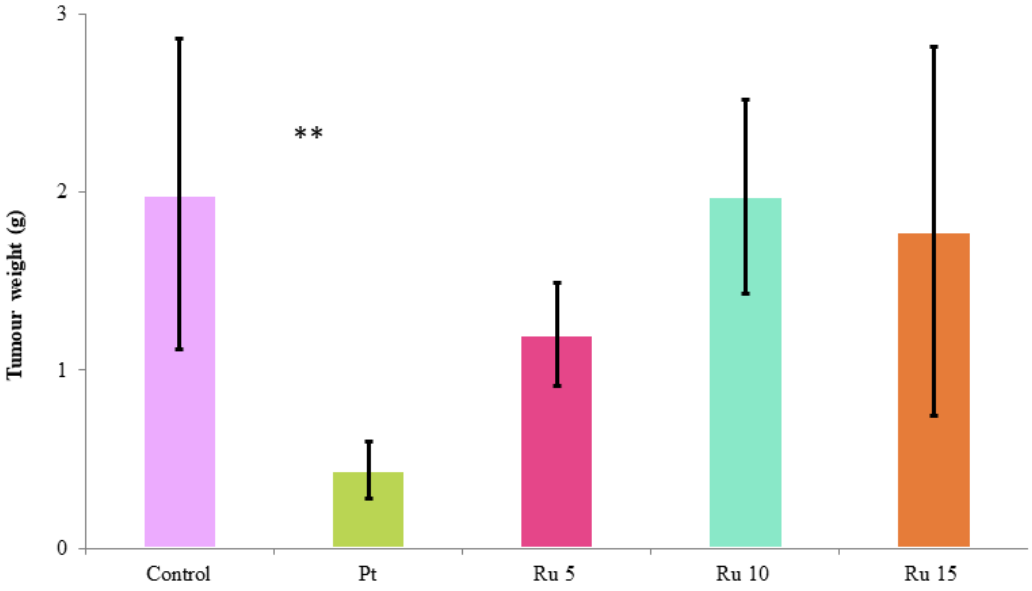


**Figure 7.** The weight of the solid Ehrlich tumour (in grams) on day 10 of mice injected on days 1 and 7 i.p. with pure vehicle, **Ru-sq** or cisplatin. Values are the means ± SEM (n = 7 in each group). Control – tumour-bearing control treated with mixture of co-solvent and water; Pt – cisplatin 5 mg/kg i.p.; Ru 5 – **Ru-sq** 5 mg/kg i.p.; Ru 10 – **Ru-sq** 10 mg/kg i.p.; Ru 15 – **Ru-sq** 15 mg/kg i.p. Significantly different from the controls (**P < 0.01).

Furthermore, the effect of **Ru-sq** on tumour growth was examined. Figure 7 shows the weight of tumours at day 10 in mice treated with mixture of co-solvent and water, **Ru-sq** at 5, 10 or 15 mg/kg, or cisplatin at 5 mg/kg, and documents differences in the effect of the used drugs. Although only cisplatin exhibited a significant inhibitory effect on tumour growth ($P = 0.0011$), there was a slight but insignificant suppression at 5 mg/kg **Ru-sq** ($P = 0.108$). As in the survival study, also here the optimum dose of **Ru-sq** seems to be in the lower part of the range tested.

**Effect of Ru-sq on the growth of A2780 human ovarian cancer in immunodeficient nude mice and survival of tumour bearing mice**

To compare the efficacy of the drug, therapeutic and survival experiment was repeated with athymic nude mice and human cancer line. A2780 human ovarian cancer cell line was chosen because of the use of cisplatin as comparative drug. Cisplatin is usually used for the therapy of ovarian cancer. Unfortunately, resistance often arises in treated patients. The use of human tumour xenografts in immunodeficient mice to examine therapeutic effect of potential chemotherapeutics, has several advantages. The major one is the use of actual human tumour tissue, featuring the complexity of genetic and epigenetic abnormalities that exist in the human tumour cell population.[94,95] We evaluated the growth of A2780 human ovarian cancer cells in immunodeficient nude mice and their survival. Figure 8 shows the survival of animals; the longest average day of death is surprisingly associated to the negative control (42.88 ± 16.97 days). However, there was one surviving mouse in the group treated with **Ru-sq** 10 mg/kg and in the group treated with cisplatin. Two surviving mice were found in the group treated with higher dose of **Ru-sq** (15 mg/kg). Very interestingly, one of them was completely cured with no observable tumour.

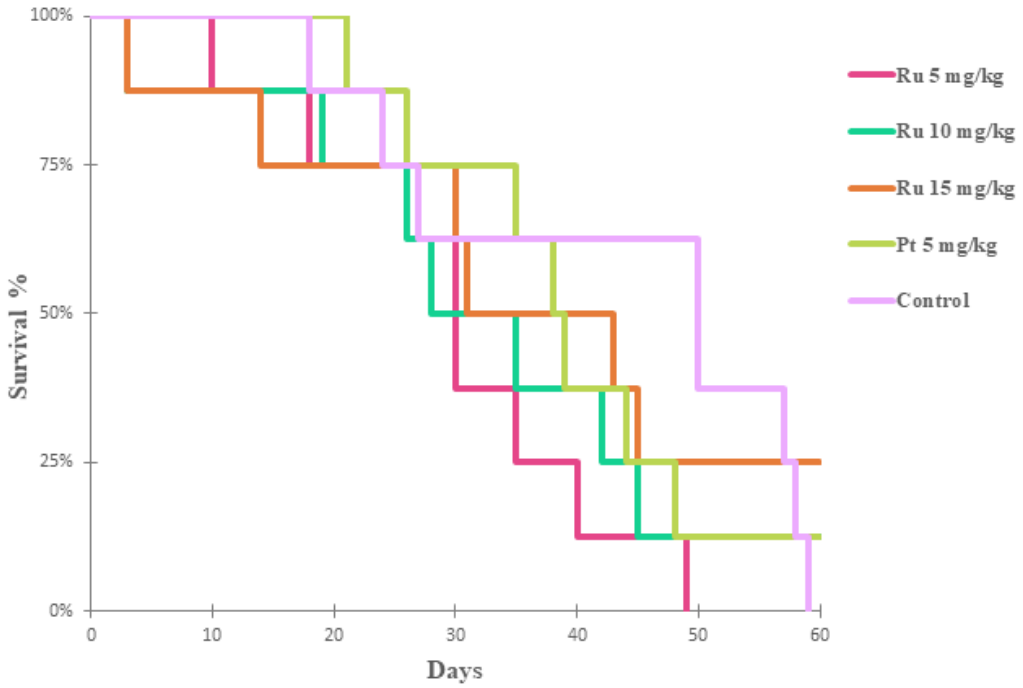


**Figure 8.** Kaplan-Meier analysis of survival of immunodeficient nude mice bearing A2780 human ovarian cancer. The treatment of Ru 15 mg/Kg led to a completely cancer free mouse. The compounds were administered i.p. on days 1 and 7 after the tumour reached 5 – 8 mm in size, n = 8 in each group.

Looking at the effect of **Ru-sq** on tumour growth (Figure 9), we observed that during the first days of therapy (day 4), there is a significant difference between groups treated with **Ru-sq** 15 mg/kg and cisplatin ($P$ = 0.00675). Similar results between these two groups were observed at days 11 and 15 ($P$ = 0,04246 for day 11 and $P$ = 0,0262 for day 15). Comparison with untreated control group showed significant differences at days 11 and 15 ($P$ = 0.024 for day 11; $P$ = 0.00931 for day 15). **Ru-sq** administered in the dose of 15 mg/kg also showed decrease in tumour size over 15 days. Very interestingly, one mouse of this group was completely cured, no tumour volume was observed on the day 36 until the end of the experiment (day 60, data not shown). The longer survival of untreated mice observed on the nude model could be rationalised by

considering the higher sensitivity of immunocompromised animals to any kind of treatment. In addition, the intraperitoneal administration of the compound itself was found not ideal because of solubility reasons, which could have led to toxic peritonitis and eventually death.

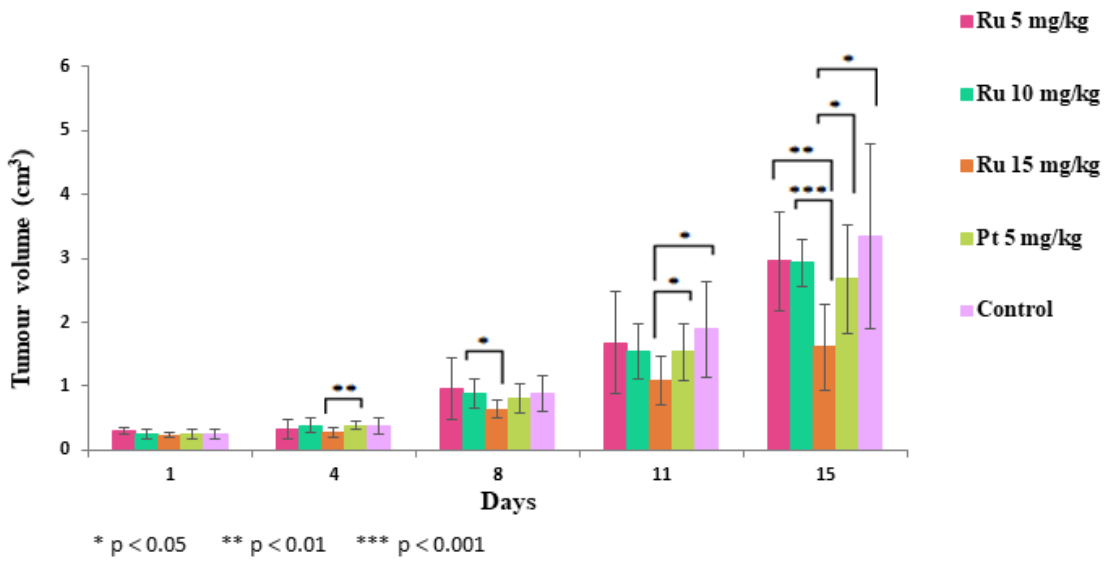


**Figure 9.** Tumour growth of A2780 cancer line in nude mice in first 15 days of therapy. Tumour size is shown as volume in $cm^3$. Control – tumour-bearing control treated with mixture of co-solvent and water; Pt – cisplatin 5 mg/kg i.p.; Ru 5 – **Ru-sq** 5 mg/kg i.p.; Ru 10 – **Ru-sq** 10 mg/kg i.p.; Ru 15 – **Ru-sq** 15 mg/kg i.p. The most significant slowing down of tumour growth is observable in the group with **Ru-sq** 15 mg/kg.

These data demonstrate that the group treated with **Ru-sq** 15 mg/kg experienced a healing effect (in some points better than cisplatin), warranting further research. **Ru-sq** in a dose of 15 mg/kg has shown great potential to be an alternative and better drug candidate than cisplatin.

Taken together, we might conclude that in both models used, **Ru-sq** reduces the growth of tumour cells and prolongs tumour-bearing mice survival in immunocompetent

NMRI mice bearing Ehrlich carcinoma. Moreover, the optimal dose would be different depending on strain of the mice and tumour type.

**Akt-1 protein levels in HeLa cells**

The interesting results obtained during the *in vivo* studies led us to further investigate the influence of **Ru-sq** on cell proliferation and/or migration. Akt is a serine/threonine kinase that promotes cellular survival.[96] Three isoforms of this protein exist in mammalian cells: Akt-1, Akt-2 and Akt-3.[97] Despite their high sequence similarity, they exhibit unique functions.[98] Akt-1 was found to be involved in the regulation of cell proliferation, transformation and tumour metastasis.[98] In this study, we assessed the influence of different concentrations of **Ru-sq** on total Akt-1 protein levels in HeLa cells. As shown in Figures 12a and 12b, the treatment with the complex at concentrations lower than the $IC_{50}$ does not change the total Akt-1 protein levels. A similar effect is observed upon treatment with cisplatin and doxorubicin at their $IC_{50}$ concentrations ($IC_{50}$ =10 and 0.3 μM, respectively for cisplatin and doxorubicin). On the other hand, Akt-1 protein levels are significantly decreasing when HeLa cells were treated with **Ru-sq** at $IC_{50}$ concentration (0.5 μM) and higher. It is important to note that GAPDH protein levels (loading control) are also changing at these concentrations, probably indicating ongoing cell death. Although **Ru-sq** complex does not change the total amount of the Akt-1 protein levels, we cannot exclude its impact on the amount of active form of this protein. It is known that Akt-1 needs to be phosphorylated for its activity[99] and hyper activation of this protein is frequently found in human cancers.[100] Further studies will be needed to fully understand the influence of our compound on cell proliferation and/or migration.

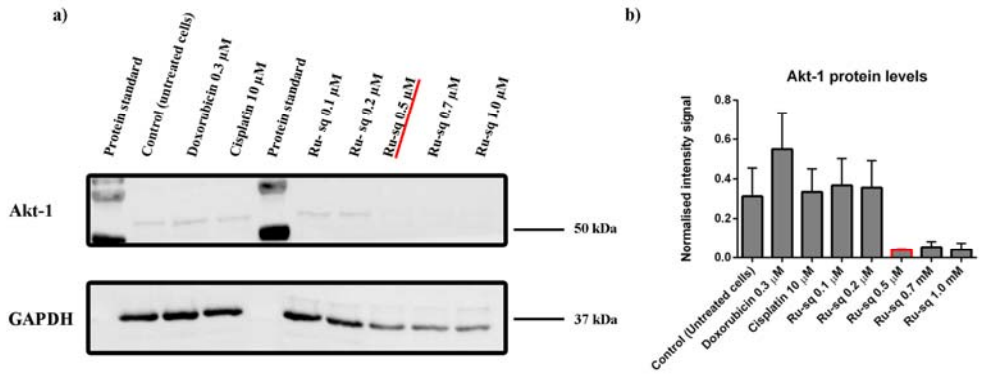


**Figure 10.** (a) Western blot analysis of Akt-1 protein levels in HeLa cell line after 24 h treatment with different concentrations of **Ru-sq**. Cisplatin, doxorubicin and untreated cells were used as controls. The positions of the nearest molecular weight markers are indicated. (b) Akt-1 protein levels normalised to GAPDH signal). Data is presented as the mean ± SD of at least 3 independent experiments. The $IC_{50}$ concentration of the complex is marked in red.

## Conclusions

**Ru-sq** was successfully synthesised and fully characterised. Crystal structure, electrochemical and EPR studies confirmed the oxidation state of the dioxo ligand (semiquinonate), which led to an overall positive charge of the complex. **Ru-sq** was found to be stable at room temperature in DMSO solution over one week and to have a half-life of 12 h upon incubation in human plasma at 37 °C. Cytotoxicity studies were performed in both, cellular monolayer (2D) and Multi Cellular Tumour Spheroids (MCTS) (3D) models. The cytotoxicity in the 2D model was tested against different cell lines showing higher activity than cisplatin with $IC_{50}$ values mostly in the nanomolar range. The cytotoxicity in HeLa MCTS confirmed the higher activity compared to cisplatin. Great tumour growth inhibition was observed after treatment with **Ru-sq** at 20 μM and 25 μM. Deeper investigation revealed apoptosis as the main cause of cell death. **Ru-sq** was found to be taken up by HeLa cells more efficiently than cisplatin and to accumulate preferentially in nucleus. DNA ruthenation studies suggest that **Ru-sq** might damage the DNA and/or prevent replication as well as transcription processes. Mitochondrial function upon **Ru-sq** treatment was also studied using an indicator of the mitochondrial membrane potential (JC-1) and mitostress test (Seahorse technology). From these studies, a severe impairement of the mitochondrial potential was observed suggesting mitochondrial disfunction contributes to the mode of action of **Ru-sq**. *In vivo* studies were performed using two different models: a syngeneic tumour growing in a naturally immunocompetent mouse, or human tumour cells growing in immunodeficient animals. **Ru-sq** reduces the growth of tumour cells and prolongs the survival of tumour-bearing mice. However, the optimal dose would be different depending on strain of the mouse and tumour type. In addition, during this study, especially in the case of the nude animals, the intraperitoneal administration was

found to be not ideal because of solubility reasons, which probably lead to some toxicity and eventually death.

Overall, **Ru-sq** displayed better activity than cisplatin in 2D and 3D cell cultures as well as for some conditions used *in vivo*. In conclusion, in this work, combining the well-known anticancer activity of Ru(II) polypyridyl complexes and the unique properties of the non-innocent ligand semiquinonate, we discovered a remarkable complex, **Ru-sq**, with promising potential as a chemotherapeutic agent against cancer. Further studies are currently ongoing in our group toward a different formulation of the compound prior administration. We hope that these studies might lead our compound to advance towards pre-clinical trials.

## Experimental Section

**Materials**.

All chemicals were either of reagent or analytical grade and used as purchased from commercial sources without additional purification. Ruthenium trichloride hydrate was provided by $I^2CNS$, 4,7-Diphenyl-1,10-phenanthroline, Lithium chloride (anhydrous, 99%), and catechol by Alfa Aesar, tetrabutylammonium hexafluorophosphate by Sigma-Aldrich. All solvents were purchased of analytical, or HPLC grade. When necessary, solvents were degassed by purging with dry, oxygen-free nitrogen for at least 30 min before use.

**Instrumentation and methods**.

Amber glass or clear glassware wrapped in tin foil were used when protection from the light was necessary. Schlenk glassware and a vacuum line were employed when reactions sensitive to moisture/oxygen had to be performed under nitrogen atmosphere. Thin layer chromatography (TLC) was performed using silica gel 60 F-254 (Merck) plates with detection of spots being achieved by exposure to UV light. Column chromatography was done using Silica gel 60-200 μm (VWR). Eluent mixtures are expressed as volume to volume (v/v) ratios. $^{1}H$ and $^{13}C$ NMR spectra were measured on Bruker Avance III HD 400 MHz or Bruker Avance Neo 500 MHz spectrometers using the signal of the deuterated solvent as an internal standard.[101] The chemical shifts $\delta$ are reported in ppm (parts per million) relative to tetramethylsilane (TMS) or signals from the residual protons of deuterated solvents. Coupling constants $J$ are given in Hertz (Hz). The abbreviation for the peaks multiplicity is br (broad). ESI-HRMS experiments were carried out using a LTQ-Orbitrap XL from Thermo Scientific (Thermo Fisher Scientific, Courtaboeuf, France) and operated in positive ionization mode, with a spray voltage at 3.6 kV. Sheath and auxiliary gas were set at a flow rate

of 5 and 0 arbitrary units (a.u.), respectively. Applied voltages were 40 and 100 V for the ion transfer capillary and the tube lens, respectively. The ion transfer capillary was held at 275°C. Detection was achieved in the Orbitrap with a resolution set to 100,000 (at m/z 400) and a m/z range between 200-2000 in profile mode. Spectrum was analysed using the acquisition software XCalibur 2.1 (Thermo Fisher Scientific, Courtaboeuf, France). The automatic gain control (AGC) allowed accumulation of up to 2.105 ions for FTMS scans, Maximum injection time was set to 300 ms and 1 μscan was acquired. 5μL was injected using a Thermo Finnigan Surveyor HPLC system (Thermo Fisher Scientific, Courtaboeuf, France) with a continuous infusion of methanol at 100 $\mu L.min^{-1}$. Purity of the compounds was determined by elemental analysis performed at Science Centre, London Metropolitan University using Thermo Fisher (Carlo Erba) Flash 2000 Elemental Analyser, configured for %CHN confirming ≥95% purity. IR spectra were recorded with SpectrumTwo FTIR Spectrometer (Perkin–Elmer) equipped with a Specac Golden GateTM ATR (attenuated total reflection) accessory; applied as neat samples; $1/\lambda$ in $cm^{-1}$. Analytical HPLC measurement was performed using the following system: 2 x Agilent G1361 1260 Prep Pump system with Agilent G7115A 1260 DAD WR Detector equipped with an Agilent Pursuit XRs 5C18 (100Å, C18 5 μm 250 x 4.6 mm) Column and an Agilent G1364B 1260-FC fraction collector. The solvents (HPLC grade) were millipore water (0.1% TFA, solvent A) and acetonitrile (0.1% TFA, solvent B). The HPLC gradient used is the following: 0-3 minutes: isocratic 90% A (5% B); 3- 25 minutes: linear gradient from 90% A (5% B) to 0% A (100% B); 25-30 minutes: isocratic 0% A (100% B), 30-35 minutes: linear gradient from 0% A (100% B) to 95% A (5% B). The flow rate was 1 mL/min. Detection was performed at 215nm, 250nm, 350nm, 450nm, 550nm and 650nm with a slit of 4nm. Stability in human plasma was performed on HPLC (Acquity Ultra

Performance LC, Waters) that was connected to a mass spectrometer (Bruker Esquire 6000) operated in ESI mode. The ACQUITY UPLC BEH C18 Gravity 1.7 μm (2.1 × 50 mm) reverse phase column was used with a flow rate of 0.6 ml/min and UV-absorption was measured at 275 nm. The runs were performed with a linear gradient of A (acetonitrile (Sigma Aldrich HPLC-grade)) and B (distilled water containing 0.1% formic acid): t = 0−0.25 min, 95% A; t = 1.5 min, 100% A; t = 2.5 min, 100% A. Fractionation ICP-MS measurements were performed on an Agilent QQQ 8800 Triple quad ICP-MS spectrometer (Agilent Technologies) with a ASX200 autosampler (Agilent Technologies), equipped with standard nickel cones and a "micro-mist" quartz nebulizer fed with 0.3 ml/min analytic flow (as a 2% $HNO_3$ aqueous solution). Celular Uptake, mechanism of uptake and ruthenation of the DNA was performed using a High-Resolution ICP-MS Element II from ThermoScientific located within the Environmental Biogeochemistry team of the Institut de Physique du Globe de Paris. This ICP-MS enables working in different resolution modes (LR=400, MR=4000 and HR=10000) for a better discrimination between elements of interest and interferences.[102]

For the metabolic studies Seahorse XFe96 Analyser by Agilent Technologies was used.

**Synthesis and characterization.**

**$Ru(DMSO)_2Cl_2$.** $Ru(DMSO)_2Cl_2$ was synthesised following an adapted literature procedure.[64] Spectroscopic data ($^1$H NMR) was in agreement with literature.[64]

**$Ru(DIP)_2Cl_2$.** The complex was synthesised following an adapted literature procedure.[65] A mixture of $Ru(DMSO)_2Cl_2$ (3.0 g, 6.19 mmol), 4,7-diphenyl-1,10-phenanthroline (4.11 g, 12.38 mmol) and LiCl (2.0 g, 47.18 mmol) dissolved in DMF (100 mL) was refluxed for 24 h. After cooling to *r.t.*, the solvent was reduced *in vacuo* to 8 mL and 350 mL of acetone were added. The mixture was then stored at -20 °C

overnight before filtration with a Buchner funnel and washed with Acetone and $Et_2O$ to afford $Ru(DIP)_2Cl_2$ as a deep purple solid (3.76 g, 4.49 mmol, 72%). Spectroscopic data ($^1H$ NMR) were in agreement with literature.[65]

**$[Ru(DIP)_2(sq)](PF_6)$ (Ru-sq).**

$Ru(DIP)_2Cl_2$ (0.739 g, 0.88 mmol) and aq. NaOH (0.5 mL, 1 M) were dissolved in 2-propanol (40 mL). The solution was degassed for 15 min and catechol (0.155 g, 1.41 mmol) was added. The mixture was heated to reflux for 24 h under $N_2$ atmosphere and protected from light. After cooling to *r.t.*, the mixture was stirred opened to air while still protected from light and the solvent was removed under vacuum. The residual solid was dissolved in 2-propanol (7 mL) and $H_2O$ (56 mL) and $NH_4PF_6$ (0.700 g, 4.3 mmol) were added. The mixture was stored in the fridge (4 °C) overnight. The precipitate was filtered with a Buchner funnel and washed with $H_2O$ (3 x 50 mL) and $Et_2O$ (3 x 50 mL). The solid was collected with DCM and dried under vacuum to deliver a crude product as the $PF_6$ salt (0.70 g), which was chromatographed on silica (DCM/MeCN 20:1 R*f*: 0.3). Evaporation of the solvent under vacuum provided $[Ru(DIP)_2(sq)](PF_6)$ as a deep red solid. Further wash with $Et_2O$ and Heptane were necessary in order to obtain clean product. The solid with the washing solvent (10 mL) was sonicated for 10 min and then centrifuged. This procedure was repeated three times for each solvent. Finally the red solid was collected with DCM and dried under vacuum to afford a clean product (0.17 g, 0.167 mmol, 19%). IR (Golden Gate, $cm^{-1}$): 3345w, 1710m, 1600w, 1520s, 1455s, 1335s, 1270s, 1125s, 820s, 760m. $^1H$ NMR (400 MHz, $CD_2Cl_2$): δ/ppm = 8.79–8.20 (br, 5H, *arom.*), 8.09–7.88 (br, 5H, *arom.*), 7.73–7.42 (br, 14H, *arom.*), 7.26–6.92 (br, 10H, *arom.*), 6.92 – 6.63 (br, 2H, *arom.*). $^{13}C$ NMR (125 MHz, $CD_2Cl_2$): δ/ppm = 149.84, 144.68, 136.10, 133.56, 130.36, 129.89, 129.53, 128.41, 126.21, 125.36, 121.47, 116.35. For the quaternary carbons, only two were

observed in the $^{13}C$ NMR spectrum where five were expected. This could be explained by peak overlap or the signal being too weak to be detected within the acquisition time of the experiment which is common for quaternary carbons. HRMS (ESI+): m/z 874.1887 $[M - PF_6]^+$. Elemental Analysis: calcd. for $C_{54}H_{36}F_6N_4O_2PRu$ = C, 63.65; H, 3.56; N, 5.50. Found = C, 63.62; H, 3.52; N, 5.45. HPLC: $T_R$ = 31.304 min.

**X-ray Crystallography**.

Single-crystal X-ray diffraction data were collected at 183(1) K on a Rigaku OD XtaLAB Synergy, Dualflex, Pilatus 200K diffractometer using a single wavelength X-ray source (Mo Kα radiation: λ = 0.71073 Å)[103] from a micro-focus sealed X-ray tube and an Oxford liquid-nitrogen Cryostream cooler. The selected suitable single crystal was mounted using polybutene oil on a flexible loop fixed on a goniometer head and transferred to the diffractometer. Pre-experiment, data collection, data reduction and analytical absorption correction[104] were performed with the program suite *CrysAlisPro*.[105] Using *Olex2*,[106] the structure was solved with the *SHELXT*[107] small molecule structure solution program and refined with the *SHELXL* program package[108] (version 2018/3) by full-matrix least-squares minimization on $F^2$. PLATON[109] was used to check the result of the X-ray analysis.

CCDC 1950873 contains the supplementary crystallographic data for this compound, and can be obtained free of charge from the Cambridge Crystallographic Data Centre via www.ccdc.cam.ac.uk/data_request/cif.

**Electrochemical Measurements**.

The electrochemical experiments were carried out with a conventional three-electrodes cell (solution volume of 15 mL) and a PC-controlled potentiostat/galvanostat (Princeton Applied Research Inc. model 263A). The working electrode was a vitreous carbon electrode from Origalys (France) exposing a geometrical area of 0.071 $cm^2$ and

mounted in Teflon®. The electrode was polished before each experiment with 3 and 0.3 μm alumina pastes followed by extensive rinsing with ultra-pure Milli-Q water. Platinum wire was used as counter electrode and saturated calomel electrode, SCE, as reference electrode. Electrolytic solutions, DMF containing tetrabutylammonium hexafluorofosfate 0.1M ($TBAPF_6$, Aldrich, +99 %) as supporting electrolyte, were routinely deoxygenated by argon bubbling. All the potential values are given versus the calomel saturated electrode SCE and recalculated versus $Me_{10}Fc^{0/+}$ potential value.

**EPR.**

Electron paramagnetic resonance (EPR) experiments were performed on a MiniScope MS400 table-top X-band spectrometer from Magnettech. Simulation of the experimental EPR spectra was performed with the MATLAB EasySpin program.[110] All samples were dissolved in dry and $N_2$-saturated DCM at a concentration of ca. 1 mM. Oxidized forms were generated using 1,1'-diacetylferrocenium hexafluoroantimonate ($Ac_2FcSbF_6$, $E_{1/2}$ = 0.940 V vs SCE in DMF/0.1 M $NBu_4PF_6$).[70,71] Chemical reduction was achieved by using cobaltocene ($Cp_2Co$, $E_{1/2}$ = -0.880 V vs SCE in DMF/0.1 M $NBu_4PF_6$). [70]

**Stability studies**.

The stability in DMSO-$d^6$ at room temperature was assessed by $^1H$ NMR over 8 days. The stability of **Ru-sq** in human plasma at 37 °C was evaluated following a slightly modified procedure already reported by our group.[43] The human plasma was provided by the Blutspendezentrum, Zurich, Switzerland. Diazepam (internal standard) was obtained from SigmaAldrich. Stock solutions of the complexes (20 mM) and diazepam (3.2 mM) were prepared in DMSO. For a typical experiment, an aliquot of the respective stock solutions and DMSO were then added to the plasma solution (975 μL)

to a total volume of 1000 µL and final concentrations of 40 µM for the complexes and diazepam. The resulting plasma solution was incubated for either: 0, 4, 6, 12, 20, 24 or 48 h at 37°C with continuous and gentle shaking (ca. 600 rpm). The reaction was stopped by addition of 2 mL of methanol, and the mixture was centrifuged for 45 min at 650g at room temperature. The methanolic solution was evaporated and the residue was suspended in 500 µL of 1:1 (v/v) acetonitrile/$H_2O$ solution. The suspension was filtered and analyzed using UPLC−MS with a total injection volume of 2 µL.

**Cell culture.**

HeLa and CT-26 cell lines were cultured in DMEM media (Gibco). CT-26 LUC cell line was cultured in DMEM media (Gibco) supplemented with 1.6 mg/mL of Genticin. RPE-1 cell line was cultured in DMEM/F-12 media (Gibco). MRC-5 cell line was cultured in DMEM/F-10 media (Gibco). A2780, A2780 cis, A2780 ADR cell lines were cultured in RPMI 1640 media (Gibco). The resistance of A2780 cis was maintained by cisplatin treatment (1µM) for one week every month. The cells were used in the assays after one week from the end of the treatment in order to avoid interfered results. The resistance of A2780 ADR was maintained by doxorubicin treatment (0.1 µM) once a week. Cells were used in the assays after three days post doxorubicin treatment in order to avoid interfered results. All cell lines were complemented with 10% of fetal calf serum (Gibco) and 100 U/mL penicillin-streptomycin mixture (Gibco) and maintained in humidified atmosphere at 37°C and 5% of $CO_2$.

**Cytotoxicity Assay using a 2D cellular model.**

Cytotoxicity of the tested **Ru-sq** and **$Ru(DIP)_2Cl_2$** complexes was assessed by a fluorometric cell viability assay using Resazurin (ACROS Organics). Briefly, cells

were seeded in triplicates in 96-well plates at a density of $4 \times 10^3$ cells/well in 100 µL. After 24 h, cells were treated with increasing concentrations of the ruthenium complexes. Dilutions for **Ru-sq** were prepared as follows: 2.0 mM stock in DMSO was diluted to 25 µM with media and then filtrated (0.22 µm filter VWR). For **$Ru(DIP)_2Cl_2$** 2.5 mM stock in DMF was prepared, which was further diluted to 100 µM and filtrated (0.22 µm filter VWR). After 48 h incubation, medium was removed, and 100 µL of complete medium containing resazurin (0.2 mg/mL final concentration) was added. After 4 h of incubation at 37 °C, the fluorescence signal of resorufin product was read (ex: 540 nm em: 590 nm) in a SpectraMax M5 microplate Reader. $IC_{50}$ values were then calculated using GraphPad Prism software.

**Generation of 3D HeLa MCTS.**

MCTS were cultured using ultra-low attachment 96 wells plates from Corning® (Fisher Scientific 15329740). HeLa cells were seeded at a density of 5000 cells per well in 200 µL. The single cells would generate MCTS approximately 400 µm in diameter at day 4 with 37 °C and 5 % $CO_2$.

**Treatment of 3D HeLa MCTS.**

HeLa MCTS after 4 days of growing at 37 °C and 5 % $CO_2$ were treated by replacing half of the medium in the well with increasing concentration of compounds for 48 h in the dark. For untreated reference MCTS, half of the medium was replaced by fresh medium only. The cytotoxicity was measured by ATP concentration with CellTiter-Glo® Cell viability kit (Promega, USA).

**CellTiter Glo® viability Test.**

Cell viability for MCTS was performed *via* ATP assay using luciferase. CellTiter-Glo® kit from Promega was used. The spheroids were incubated for 1 h after replacing half of the media with CellTiter-Glo reagent and the luminescence of the plate was read by SpectraMax M5 microplate reader. $IC_{50}$ values were calculated using GraphPad Prism software.

**HeLa MCTS growth inhibition.**

MCTS were grown and treated as previously described (see above). MCTS sizes were observed under a light microscope and pictures were taken with a Samsung Galaxy A5 2017 SM-A520FZKAXEF thanks to a phone microscope adaptor. Before imaging, the plate was sheken and half of the media was exchanged to remove dead cells. Images were recorded before treatment (day 0) and at day 3, 6, 9 and 13 after treatment. Pictures were first processed using GIMP a cross-platform image editor with a batch automation plug-in. The MCTS sizes were then calculated with SpheroidSizer, a MATLAB-based and open-source software application to measure the size of tumour spheroids automatically and accurately. Data analysis was done using GraphPad Prism software.

**Annexin V / PI assay**

Apoptosis and necrosis induction in HeLa cells treated with **Ru-sq** was evaluated *via* an AnnexinV/PI staining assay using flow cytometry. Briefly, cells were seeded at density of $2\times10^6$ cells in 10 cm cell culture dish 24 h prior cell treatments. The medium was removed and replaced with 10 µM solution of **Ru-sq** or 1 µm Staurosporin (positive control -Abcam Cat no.120056) and further incubated for 30 min, 4 h or 24 h. Cells were collected, washed twice with ice cold PBS and resuspended in 1x Annexin V binding buffer (10 x buffer composition: 0,1 M HEPES (pH 7.4), 1.4 M NaCl. 25

mM $CaCl_2$). Samples were processed according to the manufacturer instructions (BD Scientific, cat no 556463 and 556419) and analysed using ZE5 Biorad instrument at Cytometry Platform at Institute Curie. Data were analysed using the FlowJo software.

**Sample Preparation for cellular uptake**

Cells were seeded at density of $2\times10^6$. Next day, cells were treated with 5 μM concentration of **Ru-sq** or cisplatin. After 2 h, cells were collected, counted and snap frozen in liquid nitrogen and stored at -20 ºC. ICP-MS samples were prepared as follows: samples were digested using 70% nitric acid (1 mL, 60 ºC, overnight). Samples were then further diluted 1:100 (1% HCl solution in MQ water) and analysed using ICP-MS.

**Sample Preparation for cellular fractionation**

HeLa cells were seeded in three 15 $cm^2$ cell culture dishes so that on the day of treatment cells were 90% confluent. On the day of treatment cells were incubated with the target complex at a concentration of 5 μM for 2 h. After that time, the medium was removed; cells were washed, collected and counted. After resuspension in cold PBS, the organelles were isolated via different protocols (one cell culture dish per isolation was used).

*Mitochondria isolation:* To isolate mitochondria, a Mitochondria Isolation Kit (Cat. Nr: MITOISO2, Sigma Aldrich) was used according to the manufacturer procedure for isolation of mitochondria *via* homogenization method.

*Lysosome isolation:* To isolate lysosomes, a Lysosome Isolation Kit (Cat. Nr: LYSISO1, Sigma Aldrich) was used, according to the manufacturer procedure for isolation of lysosomes *via* Option C.

*Nuclear and cytoplasm isolation:* To isolate nuclear and cytoplasmic fractions, the ROCKLAND nuclear extract protocol was used.[111] Briefly cells were collected by centrifugation, resuspended in cytoplasmic extraction buffer and incubated on ice. The tubes were centrifuged and supernatant (CE) was removed. Pellets were washed with cytoplasmic extraction buffer without detergent and centrifuged. The pellet (NE) was resuspended in nuclear extraction buffer and incubated on ice. Both CE and NE were centrifuged. Supernatant from CE samples was indicated as cytoplasmic extract, whereas the pellet obtained from NE samples was indicated as nuclear extract.

ICP-MS samples were prepared as follows: isolated cellular fractions were lyophilised and digested using 5 mL of 70% nitric acid (60 ºC, overnight). Samples were then further diluted (1:1000 for nuclear pellet samples and 1:100 for all the other samples) MQ water (containing in 1% HCl solution) and analysed using ICP-MS.

**Sample preparation for studies on the mechanism of cellular uptake**

HeLa cells were seeded at density of $2\times10^6$ and next day were pre-treated with corresponding inhibitors or kept at specific temperature for 1 h. Next, cells were washed with PBS and were incubated with 5 μM of **Ru-sq** for 2 h (low temperature sample was still kept at 4 ºC). Afterwards cells were washed with PBS, collected, counted and snap frozen in liquid nitrogen. Pellets were stored at -20 ºC. ICP-MS samples were prepared as follows: samples were digested using 70% nitric acid (1 mL, 60 ºC, overnight), further diluted 1:100 (1% HCl solution in MQ water) and analysed using ICP-MS.

**DNA metalation of HeLa cells**

Cells were seeded at density of 2 x $10^6$. The following day, cells were treated with 5 μM concentration of **Ru-sq** or cisplatin. After 2 h, cells were collected, snap frozen in

liquid nitrogen and stored at -20 ºC. The following day, DNA was extracted using a PureLink™ Genomic DNA Mini Kit (Invitrogen). DNA purity was checked by absorbance measurements at 260 and 280 nm. Concentrations of genomic DNA were calculated assuming that one absorbance unit equals 50 µg/mL. ICP-MS samples were prepared as follows: samples were digested using 70% nitric acid (60 ºC, overnight) in 1:1.6 DNA to acid volume ratio. Samples were then further diluted 1:10 or 1:100 (1% HCl solution in MQ water) and analysed using ICP-MS.

**ICP-MS studies**

All ICP-MS measurements were performed on an high resolution ICP-MS (Element II, ThermoScientific) located at the Institut de physique du globe de Paris (France). The monitored isotopes are $^{101}$Ru and $^{195}$Pt. Daily, prior to the analytical sequence, the instrument was first tuned to produce maximum sensitivity and stability while also maintaining low uranium oxide formation (UO/U ≤ 5%). The data were treated as follow: intensities were converted into concentrations using uFREASI (user-FRiendly Elemental dAta proceSsIng ).[112] This software, made for HR-ICP-MS users community, is free and available on http://www.ipgp.fr/~tharaud/uFREASI.

**ICP-MS data analysis**

*Cellular uptake studies:* The amount of metal detected in the cell samples was transformed from ppb into µg of metal. Data were subsequently normalised to the number of cells and expressed as µmol of metal/ amount of cells.

*Cellular fractionation:* The amount of detected ruthenium in the cell samples was transformed from ppb into µg of ruthenium. Values were then normalised to the number of cells used for specific extraction. Due to low yield of lysosome extraction (only

25%), the values obtained were multiplied by the factor of 4. Because of a low yield of mitochondria extraction (50% of the cells were homogenized), the values obtained for that organelle were multiplied by the factor of 2. Extraction protocols allow for the isolation of pure subcellular fractions. Therefore, the total amount of metal found in the cells was calculated summing the values obtained for the pure organelles.

*Mechanism of uptake:* The amount of ruthenium detected in cell samples was transformed from ppb into μg of ruthenium and values obtained were normalised to the number of cells used for specific treatment. The value for the ruthenium found in the 37 ºC sample was used as a 100%.

*Cellular metalation:* The amount of ruthenium detected in cell samples was transformed from ppb into μg of ruthenium and value obtained was normalised to the amount of DNA.

**JC-1 Mitochondrial Membrane Potential Test.**

HeLa cells were seeded at a density of 6000 cells/ well in black 96 well-plate (costar 3916). The next day, the cells were treated with different concentrations of **Ru-sq** and **$Ru(DIP)_2Cl_2$**. After further 24 h, the cells were treated according to the JC-1 Mitochondrial Membrane Potential Assay Kit (Abcam, ab113850). The data were analysed using GraphPad Prism software.

**Mito Stress Test.**

HeLa cells were seeded in Seahorse XFe96 well plates at a density of 30,000 cells/ well in 80 μL. After 24 h, the media was replaced with fresh media and cisplatin (10 μM), catechol (10 μM), DIP (1 μM), complex **$Ru(DIP)_2Cl_2$** (10 μM) or complex **Ru-sq** (1 μM) were added. After 24 h of incubation, the regular media was removed and the cells

were washed thrice using bicarbonate and serum free DMEM, supplemented with glucose, 1.8 mg/ mL; 1% glutamine and 1% sodium pyruvate and incubated in a non-$CO_2$ incubator at 37 °C for 1 h. Mito Stress assay was run using Oligomycin, 1 μM, FCCP 1 μM and mixture of Antimycin-A/ Rotenone 1 μM each in ports A, B and C respectively using Seahorse XFe96 Extracellular Flux Analyzer.

**Glycolysis Stress Test.**

HeLa cells were seeded in Seahorse XFe96 well plates at a density of 30,000 cells/ well in 80 μL. After 24 h, the media was replaced with fresh media and cisplatin (10 μM), catechol (10 μM), DIP (1 μM), complex **$Ru(DIP)_2Cl_2$** (10 μM) or complex **Ru-sq** (1 μM) were added. After 24 h of incubation, the regular media was removed and the cells were washed thrice using bicarbonate, glucose and serum free DMEM, supplemented 1% glutamine and 1% sodium pyruvate and incubated in a non-$CO_2$ incubator at 37 °C for an hour. Glycolytic stress test was run using glucose, 10 mM, Oligomycin, 1 μM and 2-Deoxyglucose, 50 mM in ports A, B and C respectively using Seahorse XFe96 Extracellular Flux Analyzer.

**Mito Fuel Flex Test.**

HeLa cells were seeded in Seahorse XFe96 well plates at a density of 30,000 cells/ well in 80 μL. After 24 h, the media was replaced with fresh media and cisplatin (10 μM), catechol (10 μM), DIP (1 μM), complex **$Ru(DIP)_2Cl_2$** (10 μM) or complex **Ru-sq** (1 μM) were added. After 24 h of incubation, the regular media was removed and the cells were washed thrice using bicarbonate, and serum free DMEM, supplemented with 1.8 mg/mL glucose, 1% glutamine and 1% sodium pyruvate and incubated in a non-$CO_2$ incubator at 37 °C for an hour. Fuel flex assay for the different fuel pathways viz. glucose, glutamine and fatty acid was studied by measuring the basal oxygen

consumption rates and that after addition of the inhibitor of the target pathway in port A and a mixture of the inhibitors of the other two pathways in port B. This gave a measure of the dependency of the cells on a fuel pathway. To study the capacity of a certain fuel pathway, the sequence of addition of the inhibitors was reversed. In port A was added the mixture of inhibitors for the other pathways and in port B was added the inhibitor for the target pathway. UK-5099 (pyruvate dehydrogenase inhibitor, 20 μM) was used as an inhibitor for the glucose pathway. BPTES (selective inhibitor of Glutaminase GLS1, 30 μM) was used as an inhibitor for the glutamine pathway. Etomoxir (O-carnitine palmitoyltransferase-1 (CPT-1) inhibitor, 40 μM) was used as an inhibitor for the fatty acid pathway.

**Animals and Tumour Model for Ehrlich mammary carcinoma in immunocompentent NMRI mice.**

Due to the poor solubility of Ru-sq in water, dimethyl sulfoxide (DMSO), 1.81 mL / kg of body weight, had to be added to water for injections, for which reason the i.p. route of administration was chosen rather than i.v. Female outbred mice (NMRI) were used for this study, they were obtained from Masaryk University (Brno, Czech Republic). Animal care was conformed to EU recommendations and in accordance with the European convention for the protection of vertebrate animals used for experimental and other scientific purposes; it was approved by the Ethical Commission of the Medical Faculty in Hradec Králové (Nr. MSMT-56249/2012-310). For the MTD assessment, two or three healthy mice per group were observed for weight loss (the limit was 10%) over 14 days after injection of the solution. For the in vivo activity study, 70 NMRI female mice, 7 weeks old and weighting in the average 31.8 g (SD = 1.27) were fed a standard diet and water ad libitum. A solid Ehrlich tumour was purchased from the Research Institute for Pharmacy and Biochemistry (VUFB) in Prague, and then

maintained in NMRI mice by periodical transplantations. The homogenised tumour tissue was inoculated subcutaneously into all mice on day 0, using 0.2 mL of 1/1 (v/v) homogenate freshly prepared in isotonic glucose solution. The tumour-bearing mice were then divided into 5 groups of 14 animals as follows: a control group treated with the pure solvent (DMSO and water), 3 groups of animals treated with Ru-sq in doses of 5, 10, and 15 mg/kg i.p. and a positive controls receiving 5 mg/kg cisplatin i.p. (Cisplatin 50 ml/25 mg, EBEWE Pharma, Austria). The solutions were administered on days 1 and 7 in volumes of 0.2 mL per 20 g body weight. On the tenth day, half of the mice were sacrificed, and their tumours were weighed. The remaining animals were left in order to observe their survival.

**Statistical Analysis for Ehrlich mammary carcinoma in immunocompentent NMRI mice.**

One-Way Analysis of Variance with post-hoc Dunnetts's multiple comparison test was used to detect differences in tumour weight. Kaplan-Meier curves and logrank tests were used to compare survival times in groups. Here, the level of significance was $\alpha$=0.05. MS Excel 2003 and NCSS software was used for the calculations and statistical evaluations.

**Animals and Tumour Model for A2780 human ovarian cancer in immunodeficient nude mice.**

The animal experiment depicted here after were performed in accordance with the Act on Experimental Work with Animals (Public Notice of the Ministry of Agriculture of the Czech Republic No. 246/1992, No. 311/1997, No. 207/2004; Decree of the Ministry of the Environment of the Czech Republic No. 117/1987; and Act of the Czech National

Assembly No. 149/2004), which is fully compatible with the corresponding European Union directives. Athymic nude mice were used for experiment (obtained from AnLab Ltd., Prague, Czech Republic, females, 8 weeks old, n = 40). After acclimatization, the A2780 human ovarian cancer cell line was implanted subcutaneously in the shaved right flank of mice (obtained from Sigma-Aldrich, Missouri, USA, used medium RPMI with 10 % fetal bovine serum, 2x106 cells per mouse applicated with cells to Matrigel ratio 2:1). The animals were randomly divided into five groups (n = 8), when tumour reached the size of 5 – 8 mm in diameter. 5 % DMSO (dimethyl sulfoxide) solution containing Ru-sq 5 mg/kg, 10 mg/kg or 15 mg/kg (in volume 200 µl per 20 g of mouse weight) were administered intraperitoneally to the first three groups (day 1). Another group received cisplatin (5 mg/kg) in the same manner as positive control. The last group (as negative untreated control) received intraperitoneally 5 % solution of DMSO with physiologic solution. The application of all substances was repeated on day 7 of therapy. The animals were observed 60 days from first application, tumor growth, weight of mice and survival were monitored in regular intervals. The mice had free access to water and food ad libitum throughout the experiment. At the end of experiment (after 60 days) all surviving mice were sacrificed by using of overdose of intramuscular anesthetic.

**Statistical Analysis for A2780 human ovarian cancer in immunodeficient nude mice.**

One-Way Analysis of Variance with post-hoc Dunnetts's multiple comparison test was used to detect differences in tumour weight. Kaplan-Meier curves and logrank tests were used to compare survival times in groups. Here, the level of significance was

α=0.05. MS Excel 2016 and OriginPro 8 software was used for the calculations and statistical evaluations.

**Western Blot analysis of Akt-1 protein levels in HeLa cells.**

HeLa cells were seeded on a 10 cm dish so that, at the time of the treatment, cells were confluent. The next day, the cells were treated for 24 h with the compounds. After that time, the cells were collected, counted, snap frozen in liquid nitrogen and then stored at -20 ºC. Samples were then lysed in 4x SB buffer in reducing conditions, so that 10 µL of the sample contained 100 000 cells. Samples were passaged ten times through 5 mL syringe with narrow needle then were boiled for 10 min. Samples were then loaded on 10% SDS-PAGE gels (10 µL). Proteins were then blotted on a nitrocellulose membrane (Amersham Protran 0.2). Detection of Akt-1 and GAPDH proteins was conducted using following primary antibodies: anti-GAPDH (1:10000 sigma-aldrich G9545) and anti-Akt-1 (B-1) (1:50 Santa Cruz Biotechnology sc-5298). Images were taken using ChemiDoc Touch Imaging System by Biorad. Image with non-saturated bands allowed for normalization in Fiji software.

**Acknowledgements**

This work was financially supported by an ERC Consolidator Grant PhotoMedMet to G.G. (GA 681679) and has received support under the program *Investissements d'Avenir* launched by the French Government and implemented by the ANR with the reference ANR-10-IDEX-0001-02 PSL (G.G.). This work was financed by the Swiss National Science Foundation (Professorships N° PP00P2_133568 and PP00P2_157545 to G.G.), the University of Zurich (G.G), the Novartis Jubilee Foundation (G.G and R.R.), the Forschungskredit of the

University of Zurich (R.R.), the UBS Promedica Stiftung (G.G and R.R.) and the Charles University program Progres Q40/01. Ile de France Region is gratefully acknowledged for financial support of 500 MHz NMR spectrometer of Chimie-ParisTech in the framework of the SESAME equipment project. We acknowledge the loan of Agilent's equipment to Chimie ParisTech. Part of this work was supported by IPGP multidisciplinary program PARI and by Region Île-de-France SESAME Grant no. 12015908. Stefano Ferrari is supported by a grant of the Czech Science Foundation (17-02080S). Part of this work was supported by IPGP multidisciplinary program PARI and by Region Île-de-France SESAME Grant no. 12015908.

**List of Abbreviations**

A2780, human ovarian carcinoma; A2780 ADR, human doxorubicin resistant ovarian carcinoma; A2780 cis, human cisplatin resistant ovarian carcinoma; Akt, serine/threonine kinase; cat, catecholate; CT-26, mouse colon adenocarcinoma; CT-26 LUC, mouse colon adenocarcinoma stably expressing luciferase; CV, Cyclic voltammetry; DIP, 4,7-diphenyl-1,10-phenanthroline; $E_{1/2}$, Half wave potential; ECAR, extracellular acidification rate; FCCP, Carbonyl cyanide 4-(trifluoromethoxy)phenylhydrazone; GAPDH, Glyceraldehyde 3-phosphate dehydrogenase; GL-15, human glioblastoma; HeLa, human cervical adenocarcinoma; ICP-MS, Inductively Coupled Plasma Mass Spectrometry; JC-1, 5,5',6,6'-Tetrachloro-1,1',3,3'-tetraethylbenzimidazolylcarbocyanine iodide; MCTS, Multi Cellular Tumour Spheroids; MeCN, acetonitrile; MRC-5, human normal lung fibroblast; N2a, mouse neuroblastoma; NER, nucleotide excision repair; OCR, oxygen consumption rate; PAINS, pan-assay interference compounds; PDT, Photodynamic therapy; PI, propidium

iodide; q, quinone; RDE, Rotating disc electrode voltammetry; RPE-1, human normal retina pigmented epithelial; SCE, Saturated calomel electrode; sq, semiquinonate; UPLC, ultra-high-pressure liquid chromatography.

**Supporting Information**

The Supporting Information is at DOI: XXXXX.

NMR spectra and HPLC chromatograms of Ru-sq (Figure S1), crystallographic data of [Ru(DIP)2(sq)](Cl) (Figure S2), selected bond lengths and angles of Ru-1 molecule (Table S1), selected bond lengths and angles of Ru-2 molecule (Table S2), CV and RDE spectra of Ru-sq (Figure S3), electrochemical data for Ru-sq (Table S3), EPR spectra of Ru-sq (a), its reduced for Ru-sq- (b), and its oxidized form Ru-sq+ (c) (Figure S4), overlap of 1H spectra of Ru-sq in DMSO over 8 days (Figure S5), UV traces of UPLC analysis of Ru-sq (Figure S6a) percentage concentration of Ru-sq over time (Figure S6b), fluorometric cell viability assay (Figure S7), cellTiter Glo® viability Test (Figure S8), cell Death Mechanism (Figure S9), cellular uptake mechanism (Figure S10), oxygen consumption rates and different respiration parameters in HeLa cells (Figure S11), extracellular acidification rate and different parameters of glycolytic respiration in HeLa cells (Figure S12), fuel flex assay in HeLa cells (Figure S13).

**References**


(1) Urruticoechea, A.; Alemany, R.; Balart, J.; Villanueva, A.; Viñals, F.; Capellá, G. Recent Advances in Cancer Therapy: An Overview. *Curr. Pharm. Des.* **2010**, *16*, 3–10.

(2) Rosenberg, B.; Van Camp, L.; Krigas, T. Inhibition of Cell Division in Escherichia Coli by Electrolysis Products from a Platinum Electrode. *Nature* **1965**, *205*, 698–699.

(3) Rosenberg, B.; van Camp, L.; Grimley, E. B.; Thomson, A. J. The Inhibition of Growth or Cell Division in Escherichia Coli by Different Ionic Species of Platinum (IV) Complexes. *J. Biol. Chem.* **1967**, *242*, 1347–1352.

(4) Rosenberg, B.; Van Camp, L.; Trosko, J. E.; Mansour, V. H. Platinum Compounds: A New Class of Potent Antitumour Agents. *Nature* **1969**, *222*, 385–386.

(5) Rosenberg, B. B. Some Biological Effects of Platinum Compounds. *Platin. Met. Rev.* **1971**, *15*, 42–51.

(6) Pieter, P.; Lippard, S. J. Cisplatin and Related Drugs. *Encycl. Cancer* **1997**, *1*, 525–543.

(7) Wong, E.; Giandomenico, C. M. Current Status of Platinum-Based Antitumor Drugs. *Chem. Rev.* **1999**, *99*, 2451–2466.

(8) Lebwohl, D.; Canetta, R. Clinical Development of Platinum Complexes in Cancer Therapy: An Historical Perspective and an Update. *Eur. J. Cancer* **1998**, *34*, 1522–1534.

(9) Fricker, S. P. Metal Based Drugs: From Serendipity to Design. *Dalton Trans.* **2007**, *43*, 4903–4917.

(10) Singh, V.; Azad, G. K.; Reddy M., A.; Baranwal, S.; Tomar, R. S. Anti-Cancer Drug KP1019 Induces Hog1 Phosphorylation and Protein Ubiquitylation in Saccharomyces Cerevisiae. *Eur. J. Pharmacol.* **2014**, *736*, 77–85.

(11) Boros, E.; Dyson, P. J.; Gasser, G. Classification of Metal-Based Drugs

According to Their Mechanisms of Action. *Chem* **2020**, *6*, 41–60.

(12) Yang, G. J.; Wang, W.; Mok, S. W. F.; Wu, C.; Law, B. Y. K.; Miao, X. M.; Wu, K. J.; Zhong, H. J.; Wong, C. Y.; Wong, V. K. W.; Ma, D. L.; Leung, C. H. Selective Inhibition of Lysine-Specific Demethylase 5A (KDM5A) Using a Rhodium(III) Complex for Triple-Negative Breast Cancer Therapy. *Angew. Chem. Int. Ed.* **2018**, *57*, 13091–13095.

(13) Ndagi, U.; Mhlongo, N.; Soliman, M. E. Metal Complexes in Cancer Therapy – An Update from Drug Design Perspective. *Drug Des. Devel. Ther.* **2017**, *11*, 599–616.

(14) Vellaisamy, K.; Li, G.; Wang, W.; Leung, C. H.; Ma, D. L. A Long-Lived Peptide-Conjugated Iridium(Iii) Complex as a Luminescent Probe and Inhibitor of the Cell Migration Mediator, Formyl Peptide Receptor 2. *Chem. Sci.* **2018**, *9*, 8171–8177.

(15) Ma, W.; Guo, L.; Tian, Z.; Zhang, S.; He, X.; Li, J.; Yang, Y.; Liu, Z. Rhodamine-Modified Fluorescent Half-Sandwich Iridium and Ruthenium Complexes: Potential Application as Bioimaging and Anticancer Agents. *Dalton Trans.* **2019**, *48*, 4788–4793.

(16) Ma, W.; Ge, X.; Guo, L.; Zhang, S.; Li, J. J.; He, X.; Liu, Z. Bichromophoric Anticancer Drug: Targeting Lysosome with Rhodamine Modified Cyclometalated Iridium(III) Complexes. *Dyes Pigm.* **2019**, *162*, 385–393.

(17) Li, J.; Guo, L.; Tian, Z.; Zhang, S.; Xu, Z.; Han, Y.; Li, R.; Li, Y.; Liu, Z. Half-Sandwich Iridium and Ruthenium Complexes: Effective Tracking in Cells and Anticancer Studies. *Inorg. Chem.* **2018**, *57*, 13552–13563.

(18) He, L.; Tan, C. P.; Ye, R. R.; Zhao, Y. Z.; Liu, Y. H.; Zhao, Q.; Ji, L. N.; Mao, Z. W. Theranostic Iridium(III) Complexes as One- and Two-Photon Phosphorescent Trackers to Monitor Autophagic Lysosomes. *Angew. Chem. Int. Ed.* **2014**, *53*, 12137–12141.

(19) Allardyce, B. C. S.; Dyson, P. J. Ruthenium in Medicine: Current Clinical Uses and Future Prospects. *Platin. Met. Rev.* **2001**, *45*, 62–69.

(20) Antonarakis, E. S.; Emadi, A. Ruthenium-Based Chemotherapeutics: Are They Ready for Prime Time? *Cancer Chemother. Pharmacol.* **2010**, *66*, 1–9.

(21) Pongratz, M.; Schluga, P.; Jakupec, M. A.; Arion, V. B.; Hartinger, C. G.; Allmaier, G.; Keppler, B. K. Transferrin Binding and Transferrin-Mediated Cellular Uptake of the Ruthenium Coordination Compound KP1019, Studied by Means of AAS, ESI-MS and CD Spectroscopy. *J. Anal. At. Spectrom.* **2004**, *19*, 46–51.

(22) Alessio, E. Thirty Years of the Drug Candidate NAMI-A and the Myths in the Field of Ruthenium Anticancer Compounds: A Personal Perspective. *Eur. J. Inorg. Chem.* **2017**, *55*, 1549–1560.

(23) Thota, S.; Rodrigues, D. A.; Crans, D. C.; Barreiro, E. J. Ru(II) Compounds: Next-Generation Anticancer Metallotherapeutics? *J. Med. Chem.* **2018**, *61*, 5805–5821.

(24) Notaro, A.; Gasser, G. Monomeric and Dimeric Coordinatively Saturated and Substitutionally Inert Ru(II) Polypyridyl Complexes as Anticancer Drug Candidates. *Chem. Soc. Rev.* **2017**, *46*, 7317–7337.

(25) Hartinger, C. G.; Jakupec, M. a; Zorbas-Seifried, S.; Groessl, M.; Egger, A.; Berger, W.; Zorbas, H.; Dyson, P. J.; Keppler, B. K. KP1019, a New Redox-Active Anticancer Agent--Preclinical Development and Results of a Clinical Phase I Study in Tumor Patients. *Chem. Biodivers.* **2008**, *5*, 2140–2155.

(26) Shum, J.; Leung, P. K.; Lo, K. K. Luminescent Ruthenium(II) Polypyridine Complexes for a Wide Variety of Biomolecular and Cellular Applications. *Inorg. Chem.* **2019**, *58*, 2231–2247.

(27) Patra, M.; Gasser, G. Organometallic Compounds: An Opportunity for Chemical Biology? *ChemBioChem* **2012**, *13*, 1232–1252.

(28) Dörr, M.; Meggers, E. Metal Complexes as Structural Templates for Targeting Proteins. *Curr. Opin. Chem. Biol.* **2014**, *19*, 76–81.

(29) Jakubaszek, M.; Goud, B.; Ferrari, S. Mechanisms of Action of Ru ( II ) Polypyridyl Complexes in Living Cells upon Light Irradiation. *Chem. Commun.*

**2018**, *54*, 13040–13059.

(30) Sava, G.; Capozzi, I.; Clerici, K.; Gagliardi, G.; Alessio, E.; Mestroni, G. Pharmacological Control of Lung Metastases of Solid Tumours by a Novel Ruthenium Complex. *Clin. Exp. Metastasis* **1998**, *16*, 371–379.

(31) Lentz, F.; Drescher, A.; Lindauer, A.; Henke, M.; Hilger, R. a; Hartinger, C. G.; Scheulen, M. E.; Dittrich, C.; Keppler, B. K.; Jaehde, U. Pharmacokinetics of a Novel Anticancer Ruthenium Complex (KP1019, FFC14A) in a Phase I Dose-Escalation Study. *Anticancer. Drugs* **2009**, *20*, 97–103.

(32) Trondl, R.; Heffeter, P.; Kowol, C. R.; Jakupec, M. a.; Berger, W.; Keppler, B. K. NKP-1339, the First Ruthenium-Based Anticancer Drug on the Edge to Clinical Application. *Chem. Sci.* **2014**, *5*, 2925–2932.

(33) Hartinger, C. G.; Zorbas-Seifried, S.; Jakupec, M. A.; Kynast, B.; Zorbas, H.; Keppler, B. K. From Bench to Bedside - Preclinical and Early Clinical Development of the Anticancer Agent Indazolium Trans-[Tetrachlorobis(1H-Indazole)Ruthenate(III)] (KP1019 or FFC14A). *J. Inorg. Biochem.* **2006**, *100*, 891–904.

(34) Burris, H. A.; Bakewell, S.; Bendell, J. C.; Infante, J.; Jones, S. F.; Spigel, D. R.; Weiss, G. J.; Ramanathan, R. K.; Ogden, A.; Hoff, D. Von. Safety and Activity of IT-139 , a Ruthenium-Based Compound , in Patients with Advanced Solid Tumours : A First- Phase I Study with Expansion Cohort. *ESMO Open* **2016**, 1–8.

(35) McFarland, S. A.; Mandel, A.; Dumoulin-White, R.; Gasser, G. Metal-Based Photosensitizers for Photodynamic Therapy: The Future of Multimodal Oncology? *Curr. Opin. Chem. Biol.* **2020**, *56*, 23–27.

(36) Yin, H.; Roque, J.; Konda, P.; Monro, S.; Colo, K. L.; Gujar, S.; Thummel, R. P.; Lilge, L.; Cameron, C. G.; Mcfarland, S. A. Transition Metal Complexes and Photodynamic Therapy from a Tumor-Centered Approach : Challenges , Opportunities , and Highlights from the Development of TLD1433. *Chem. Rev.* **2019**, *119*, 797–828.

(37) Https://clinicaltrials.gov/ct2/show/NCT03945162?term=TLD-1433&rank=1.

(accessed Sept 27, 2019).

(38) Gill, M. R.; Derrat, H.; Smythe, C. G. W.; Battaglia, G.; Thomas, J. A. Ruthenium(II) Metallo-Intercalators: DNA Imaging and Cytotoxicity. *ChemBioChem* **2011**, *12*, 877–880.

(39) Deepika, N.; Shobha Devi, C.; Praveen Kumar, Y.; Laxma Reddy, K.; Venkat Reddy, P.; Anil Kumar, D.; Singh, S. S.; Satyanarayana, S. DNA-Binding, Cytotoxicity, Cellular Uptake, Apoptosis and Photocleavage Studies of Ru(II) Complexes. *J. Photochem. Photobiol. B Biol.* **2016**, *160*, 142–153.

(40) Wang, H.; Liu, Y.; Li, M.; Huang, H.; Xu, H. M.; Hong, R. J.; Shen, H. Targeting Telomeric G-Quadruplexes with the Ruthenium(II) Complexes [Ru(Bpy)2(Ptpn)]2+ and [Ru(Phen)2(Ptpn)]2+. *Dalton Trans.* **2013**, *42*, 4386–4397.

(41) Srishailam, A.; Kumar, Y. P.; Venkat Reddy, P.; Nambigari, N.; Vuruputuri, U.; Singh, S. S.; Satyanarayana, S. Cellular Uptake, Cytotoxicity, Apoptosis, DNA-Binding, Photocleavage and Molecular Docking Studies of Ruthenium(II) Polypyridyl Complexes. *J. Photochem. Photobiol. B Biol.* **2014**, *132*, 111–123.

(42) Tan, C.; Lai, S.; Wu, S.; Hu, S.; Zhou, L.; Chen, Y.; Wang, M.; Zhu, Y.; Lian, W.; Peng, W.; Ji, L.; Xu, A. Nuclear Permeable Ruthenium(II) β-Carboline Complexes Induce Autophagy to Antagonize Mitochondrial-Mediated Apoptosis. *J. Med. Chem.* **2010**, *53*, 7613–7624.

(43) Pierroz, V.; Joshi, T.; Leonidova, A.; Mari, C.; Schur, J.; Ott, I.; Spiccia, L.; Ferrari, S.; Gasser, G. Molecular and Cellular Characterization of the Biological Effects of Ruthenium(II) Complexes Incorporating 2-Pyridyl-2-Pyrimidine-4-Carboxylic Acid. *J. Am. Chem. Soc.* **2012**, *134*, 20376–20387.

(44) Jiang, G. Bin; Zheng, X.; Yao, J. H.; Han, B. J.; Li, W.; Wang, J.; Huang, H. L.; Liu, Y. J. Ruthenium(II) Polypyridyl Complexes Induce BEL-7402 Cell Apoptosis by ROS-Mediated Mitochondrial Pathway. *J. Inorg. Biochem.* **2014**, *141*, 170–179.

(45) Wang, Y. C.; Qian, C.; Peng, Z. L.; Hou, X. J.; Wang, L. L.; Chao, H.; Ji, L. N. Dual Topoisomerase i and II Poisoning by Chiral Ru(II) Complexes Containing

2-Thiophenylimidazo[4,5-f][1,10]Phenanthroline Derivatives. *J. Inorg. Biochem.* **2014**, *130*, 15–27.

(46) Kou, J. F.; Qian, C.; Wang, J. Q.; Chen, X.; Wang, L. L.; Chao, H.; Ji, L. N. Chiral Ruthenium(II) Anthraquinone Complexes as Dual Inhibitors of Topoisomerases I and II. *J. Biol. Inorg. Chem.* **2012**, *17*, 81–96.

(47) Schatzschneider, U.; Niesel, J.; Ott, I.; Gust, R.; Alborzinia, H.; Wölfl, S. Cellular Uptake, Cytotoxicity, and Metabolic Profiling of Human Cancer Cells Treated with Ruthenium(II) Polypyridyl Complexes [Ru(Bpy) 2(N-N)]Cl2 with N-N=bpy, Phen, Dpq, Dppz, and Dppn. *ChemMedChem* **2008**, *3*, 1104–1109.

(48) Ward, M. D.; Mccleverty, J. A.; Ward, M. D. Non-Innocent Behaviour in Mononuclear and Polynuclear Complexes: Consequences for Redox and Electronic Spectroscopic Properties. *J. Chem. Soc. Dalton Trans.* **2002**, 275–288.

(49) Vlček, A. Metal and Ligand Oxidation States in Dioxolene Complexes: Meaning, Assignment and Control. *Comments Inorg. Chem.* **1994**, *16*, 207–228.

(50) Pierpont, C. G. Studies on Charge Distribution and Valence Tautomerism in Transition Metal Complexes of Catecholate and Semiquinonate Ligands. *Coord. Chem. Rev.* **2001**, *217*, 99–125.

(51) Creutz, C. *Progress in Inorganic Chemistry*; Karlin, K. D., Ed.; John Wiley & Sons, Inc, 1994; Vol. 41.

(52) Haga, M.; Dodsworth, E. S.; Lever, A. B. P. Catechol-Quinone Redox Series Involving Bis (Bipyridine) Ruthenium (II) and Tetrakis (Pyridine) Ruthenium (II). *Inorg. Chem.* **1986**, *25*, 447–453.

(53) Wada, T.; Yamanaka, M.; Fujihara, T.; Miyazato, Y.; Tanaka, K. Experimental and Theoretical Evaluation of the Charge Distribution over the Ruthenium and Dioxolene Framework of [Ru(OAc)(Dioxolene)(Terpy)] (Terpy = 2,2′:6′,2″-Terpyridine) Depending on the Substituents. *Inorg. Chem.* **2006**, *45*, 8887–8894.

(54) Muckerman, J. T.; Polyansky, D. E.; Wada, T.; Tanaka, K.; Fujita, E. Water Oxidation by a Ruthenium Complex with Noninnocent Quinone Ligands:

Possible Formation of an O-O Bond at a Low Oxidation State of the Metal. *Inorg. Chem.* **2008**, *47*, 1787–1802.

(55) Jones, S. E.; Chin, D.; Sawyer, D. T. Redox Chemistry of Metal-Catechol Complexes in Aprotic Media. 2. 3,5-Di-Fert-Butylcatecholato Complexes of Manganese(IV) and Manganese(III). *Inorg Chem* **1981**, *20*, 4257–4262.

(56) Baell, J. B. Feeling Nature's PAINS: Natural Products, Natural Product Drugs, and Pan Assay Interference Compounds (PAINS). *J. Nat. Prod.* **2016**, *79*, 616–628.

(57) Lima, R. M. F.; Alvarez, L. D. G.; Costa, M. F. D.; Costa, S. L.; El-Bachá, R. S. Cytotoxic Effects of Catechol to Neuroblastoma N2a Cells. *Gen. Physiol. Biophys* **2008**, *27*, 306–314.

(58) Almeida, W. L. C.; Vítor, D. N.; Pereira, M. R. G.; De Sá, D. S.; Alvarez, L. D. G.; Pinheiro, A. M.; Costa, S. L.; Costa, M. F. D.; Da Rocha, Z. N.; El-Bachá, R. S. Redox Properties of Ruthenium Complex with Catechol Are Involved in Toxicity to Glial Cells. *J. Chil. Chem. Soc.* **2007**, *52*, 1240–1243.

(59) Lin, D.; Dai, F.; Sun, L. Di; Zhou, B. Toward an Understanding of the Role of a Catechol Moiety in Cancer Chemoprevention: The Case of Copper- and o-Quinone-Dependent Nrf2 Activation by a Catechol-Type Resveratrol Analog. *Mol. Nutr. Food Res.* **2015**, *59*, 2395–2406.

(60) Galvao de Lima, R.; Lever, A. B. P.; Ito, I. Y.; Santana da Silva, R. Antifungal Activity of Novel Catecholamine Ruthenium (III) Complexes. *Transit. Met. Chem.* **2003**, *28*, 272–275.

(61) Huong, V. T.; Shimanouchi, T.; Shimauchi, N.; Yagi, H.; Umakoshi, H.; Goto, Y.; Kuboi, R. Catechol Derivatives Inhibit the Fibril Formation of Amyloid-β Peptides. *J. Biosci. Bioeng.* **2010**, *109*, 629–634.

(62) Crans, D. C.; Koehn, J. T.; Petry, S. M.; Glover, C. M.; Wijetunga, A.; Kaur, R. Levina, A.; Lay, P. A. Hydrophobicity may enhance membrane affinity and anti-cancer effects of Schiff base vanadium(v) catecholate complexes. *Dalton Trans.* **2019**, *48*, 6383–6395.

(63) Lemons, B. G.; Richens, D. T.; Anderson, A.; Sedgwick, M.; Crans, D. C.; Johnson, M. D. Stabilization of a Vanadium(V)–Catechol Complex by Compartmentalization and Reduced Solvation inside Reverse Micelles. *New J. Chem.* **2013**, *37*, 75–91.

(64) Brastos, I.; Alessio, E.; Ringenberg, M. E.; Rauchfuss, T. B. Ruthenium Complexes. In *Inorganic Syntheses*; Rauchfuss, T. B., Ed.; 2010; Vol. 35, pp 148–163.

(65) Caspar, R.; Cordier, C.; Waern, J. B.; Guyard-Duhayon, C.; Gruselle, M.; Le Floch, P.; Amouri, H. A New Family of Mono- and Dicarboxylic Ruthenium Complexes $[Ru(DIP)_2(L2)]^{2+}$ (DIP = 4,7-Diphenyl-1,10-Phenanthroline): Synthesis, Solution Behavior, and X-Ray Molecular Structure of Trans - $[Ru(DIP)_2(MeOH)_2][OTf]_2$. *Inorg. Chem.* **2006**, *45*, 4071–4078.

(66) Carugo, O.; Castellani, C. B.; Djinovicb, K.; Rizzi, M. Ligands Derived from O-Benzoquinone : Statistical Correlation between Oxidation State and Structural Features. *J. Chem. Soc. Dalton Trans.* **1992**, *10*, 1–5.

(67) Higgins, S. L. H.; White, T. A.; Winkel, B. S. J.; Brewer, K. J. Redox, Spectroscopic, and Photophysical Properties of Ru-Pt Mixed-Metal Complexes Incorporating 4,7-Diphenyl-1,10-Phenanthroline as Efficient DNA Binding and Photocleaving Agents. *Inorg. Chem.* **2011**, *50*, 463–470.

(68) Mongelli, M. T.; Brewer, K. J. Synthesis and Study of the Light Absorbing, Redox and Photophysical Properties of Ru(II) and Os(II) Complexes of 4,7-Diphenyl-1,10-Phenanthroline Containing the Polyazine Bridging Ligand 2,3-Bis(2-Pyridyl)Pyrazine. *Inorg. Chem. Commun.* **2006**, *9*, 877–881.

(69) Medhi, O. K.; Agarwala, U. Electron Spin Resonance Studies of Some

Ruthenium(III) Complexes. *Inorg Chem.* **1980**, *1*, 1381–1384.

(70) Connelly, N. G.; Geiger, W. E. Chemical Redox Agents for Organometallic Chemistry. *Chem. Rev.* **1996**, *96*, 877−910.

(71) Bao, D.; Millare, B.; Xia, W.; Steyer, B. G.; Gerasimenko, A. A.; Ferreira, A.; Contreras, A.; Vullev, V. I. Electrochemical Oxidation of Ferrocene : A Strong Dependence on the Concentration of the Supporting Electrolyte for Nonpolar Solvents. *J. Phys. Chem. A* **2009**, *2*, 1259–1267.

(72) Frei, A.; Rubbiani, R.; Tubafard, S.; Blacque, O.; Anstaett, P.; Felgenträger, A.; Maisch, T.; Spiccia, L.; Gasser, G. Synthesis, Characterization, and Biological Evaluation of New Ru(II) Polypyridyl Photosensitizers for Photodynamic Therapy. *J. Med. Chem.* **2014**, *57*, 7280–7292.

(73) Cepeda, V.; Fuertes, M.; Castilla, J.; Alonso, C.; Quevedo, C.; Perez, J. Biochemical Mechanisms of Cisplatin Cytotoxicity. *Anticancer. Agents Med. Chem.* **2007**, *7*, 3–18.

(74) Keizer, H. G.; Pinedo, H. M.; Schuurhuis, G. J.; Joenje, H. Doxorubicin (Adriamycin): A Critical Review of Free Radical-Dependent Mechanisms of Cyototoxicity. *Pharmac. Ther.* **1990**, *47*, 219–231.

(75) Kelm, J. M.; Timmins, N. E.; Brown, C. J.; Fussenegger, M.; Nielsen, L. K. Multicellular Tumor Spheroids Applicable to a Wide Variety of Cell Types. *Biotechnol. Bioeng.* **2003**, *83*, 173–180.

(76) Ma, H.; Jiang, Q.; Han, S.; Wu, Y.; Tomshine, J. C.; Wang, D.; Gan, Y.; Zou, G. Multicellular Tumor Spheroids as an In Vivo – Like Tumor Model for Three-Dimensional Imaging of Chemotherapeutic and Nano Material Cellular Penetration. *Mol. Imaging* **2012**, *11*, 487–498.

(77) Kapałczyńska, M.; Kolenda, T.; Przybyła, Weronika Zajączkowska, Maria Teresiak, A.; Filas, V.; Ibbs, M.; Bliźniak, R.; Łuczewski, Łukasz Lamperska, K. State of the Art Paper 2D and 3D Cell Cultures – a Comparison of Different Types of Cancer Cell Cultures. *Arch. Med. Sci.* **2018**, *14*, 910–919.

(78) Friedrich, J.; Seidel, C.; Ebner, R.; Kunz-Schughart, L. A. Spheroid-Based Drug

Screen : Considerations and Practical Approach. *Nat. Protoc.* **2009**, *4*, 309–324.

(79) Hess, J.; Huang, H.; Kaiser, A.; Pierroz, V.; Blacque, O. Evaluation of the Medicinal Potential of Two Ruthenium ( II ) Polypyridine Complexes as One- and Two-Photon Photodynamic Therapy Photosensitizers. *Chem. Eur. J.* **2017**, *23*, 9888–9896.

(80) Seo, O. W.; Kim, M.; Hulme, J.; An, S. S. A. Monitoring the Effects of Doxorubicin on 3D-Spheroid Tumor Cells in Real-Time. *Onco. Targets. Ther.* **2016**, *9*, 7207–7218.

(81) Rieger, A. M.; Nelson, K. L.; Konowalchuk, J. D.; Barreda, D. R. Modified Annexin V/Propidium Iodide Apoptosis Assay For Accurate Assessment of Cell Death. *J. Vis. Exp.* **2011**, *50*, 2–5.

(82) Belmokhtar, A. C.; Hillion, J.; Ségal-Bendirdjian, E. Staurosporine Induces Apoptosis through Both Caspase-Dependent and Caspase-Independent Mechanisms. *Oncogene* **2001**, *20*, 3354–3362.

(83) Zeng, L.; Chen, Y.; Huang, H.; Wang, J.; Zhao, D.; Ji, L.; Chao, H. Cyclometalated Ruthenium(II) Anthraquinone Complexes Exhibit Strong Anticancer Activity in Hypoxic Tumor Cells. *Chem. Eur. J.* **2015**, *21*, 15308–15319.

(84) Zisowsky, J.; Koegel, S.; Leyers, S.; Devarakonda, K.; Kassack, M. U.; Osmak, M.; Jaehde, U. Relevance of Drug Uptake and Efflux for Cisplatin Sensitivity of Tumor Cells. *Biochem. Pharmacol.* **2007**, *73*, 298–307.

(85) Puckett, C. A.; Barton, J. K. Fluorescein Redirects a Ruthenium - Octaarginine Conjugate to the Nucleus. *J. Am. Chem. Soc.* **2009**, *131*, 8738–8739.

(86) Goldstein, B. M.; Barton, J. K.; Berman, H. M. Crystal and Molecular Structure of a Chiral-Specific DNA-Binding Agent: Tris(4,7-Diphenyl-1,10-Phenanthroline)Ruthenium(II). *Inorg. Chem.* **1986**, *25*, 842–847.

(87) Tsujimoto, Y. Mitochondria and Cell Death. *Cell Death Differ.* **2000**, *7*, 134–135.

(88) Dedov, V. N.; Cox, G. C.; Roufogalis, B. D. Visualisation of Mitochondria in

Living Neurons with Single- and Two-Photon Fluorescence Laser Microscopy. *Micron* **2001**, *32*, 653–660.

(89) Lv, Z.; Wei, H.; Li, Q.; Su, X.; Liu, S.; Zhang, K. Y.; Lv, W.; Zhao, Q.; Li, X.; Huang, W. Achieving Efficient Photodynamic Therapy under Both Normoxia and Hypoxia Using Cyclometalated Ru(II) Photosensitizer through Type. *Chem. Sci.* **2018**, *9*, 502–512.

(90) Zorova, L. D.; Popkov, V. A.; Plotnikov, E. Y.; Silachev, D. N.; Pevzner, B.; Jankauskas, S. S.; Babenko, V. A.; Zorov, S. D.; Balakireva, A. V; Juhaszova, M.; Sollott, S. J.; Zorov, D. B. Mitochondrial Membrane Potential. *Anal. Biochem.* **2018**, *552*, 50–59.

(91) Ly, J. D.; Grubb, D. R.; Lawen, A. The Mitochondrial Membrane Potential (Δ ψ m) in Apoptosis ; an Update. *Apoptosis* **2003**, *8*, 115–128.

(92) Sakamuru, S.; Attene-ramos, M. S.; Xia, M. Mitochondrial Membrane Potential Assay. In *High-Throughput Screening Assays in Toxicology, Methods in Molecular Biology,*; Springer Science + Business Media New York, 2016; Vol. 1473, pp 17–22.

(93) Zhen-ge, L.; Xiao-hua, R.; Sha-sha, W.; Xin-hua, L.; Ya-ling, T. Immunocompromised and Immunocompetent Mouse Models for Head and Neck Squamous Cell Carcinoma. *Onco. Targets. Ther.* **2016**, *9*, 545–555.

(94) Jung, J. Human Tumor Xenograft Models for Preclinical Assessment of Anticancer Drug Development. *Toxicol. Res.* **2014**, *30*, 1–5.

(95) Xu, C.; Li, X.; Liu, P.; Li, M. A. N.; Luo, F. Patient - Derived Xenograft Mouse Models : A High Fidelity Tool for Individualized Medicine (Review). *Oncol. Lett.* **2019**, *17*, 3–10.

(96) Clark, A. S.; West, K.; Streicher, S.; Dennis, P. A. Constitutive and Inducible Akt Activity Promotes Resistance to Chemotherapy , Trastuzumab , or Tamoxifen in Breast Cancer Cells. *Mol. Cancer Ther.* **2002**, *1*, 707–717.

(97) Zhang, J. U. N.; Zhang, L. L. I.; Shen, L. E. I.; Xu, X.; Yu, H. G. Regulation of AKT Gene Expression by Cisplatin. *Oncol. Lett.* **2013**, *5*, 756–760.

(98) Santi, S. A.; Douglas, A. C. H.; Lee. The Akt Isoforms , Their Unique Functions and Potential as Anticancer Therapeutic Targets. *BioMol Concepts* **2010**, *1*, 389–401.

(99) Manning, B. D.; Toker, A. AKT / PKB Signaling : Navigating the Network. *Cell* **2017**, *169*, 381–405.

(100) Mitchell, C.; Testa, J. R. Diverse Mechanisms of AKT Pathway Activation in Human Malignancy. *Curr. Cancer Drug Targets* **2013**, *13*, 234–244.

(101) Fulmer, G. R.; Miller, A. J. M.; Sherden, N. H.; Gottlieb, H. E.; Nudelman, A.; Stoltz, B. M.; Bercaw, J. E.; Goldberg, K. I. NMR Chemical Shifts of Trace Impurities: Common Laboratory Solvents, Organics, and Gases in Deuterated Solvents Relevant to the Organometallic Chemist. *Organometallics* **2010**, *29*, 2176–2179.

(102) Krachler, M. Environmental Applications of Single Collector High Resolution ICP-MS. *J. Environ. Monit.* **2007**, *9*, 790–804.

(103) Rigaku Oxford Diffraction Ltd, Yarnton, England.

(104) Clark, R. C.; Reid, J. S. The Analytical Calculation of Absorption in Multifaceted Crystals. *Acta Crystallogr. Sect. A* **1995**, *51*, 887–897.

(105) Rigaku OD (2015). CrysAlis PRO, version 1.171.39.9f. Rigaku Oxford Diffraction Ltd, Yarnton, England.

(106) Dolomanov, O. V.; Bourhis, L. J.; Gildea, R. J.; Howard, J. A. K.; Puschmann, H. OLEX2: A Complete Structure Solution, Refinement and Analysis Program. *J. Appl. Crystallogr.* **2009**, *42*, 339–341.

(107) Sheldrick, G. M. SHELXT - Integrated Space-Group and Crystal-Structure Determination. *Acta Crystallogr. Sect. A Found. Adv.* **2015**, *71*, 3–8.

(108) Sheldrick, G. M. Crystal Structure Refinement with SHELXL. *Acta Crystallogr. Sect. C Struct. Chem.* **2015**, *71*, 3–8.

(109) Spek, A. L. Single-Crystal Structure Validation with the Program PLATON. *J. Appl. Crystallogr.* **2003**, *36*, 7–13.

(110) Stoll, S.; Schweiger, A. EasySpin , a Comprehensive Software Package for Spectral Simulation and Analysis in EPR. *J. Magn. Reson.* **2006**, *178*, 42–55.

(111) Https://rockland-inc.com/Nuclear-Extract-Protocol.aspx. (accessed Oct 3, 2019).

(112) Tharaud, M.; Gardoll, S.; Khelifi, O.; Benedetti, M. F.; Sivry, Y. UFREASI: User-FRiendly Elemental DAta ProcesSIng. A Free and Easy-to-Use Tool for Elemental Data Treatment. *Microchem. J.* **2015**, *121*, 32–40.

**Table of Contents graphic**

A ruthenium (II) polypyridyl complex bearing a non-innocent dioxo ligand demonstrates an impressive potential as a chemotherapeutic agent against cancer both *in vitro* and *in vivo*.